JGR Atmospheres

RESEARCH ARTICLE
10.1029/2020JD033439

The Global Budget of Atmospheric Methanol: New Constraints on Secondary, Oceanic, and Terrestrial Sources

Kelvin H. Bates[1], Daniel J. Jacob[1], Siyuan Wang[2], Rebecca S. Hornbrook[2], Eric C. Apel[2], Michelle J. Kim[3,4], Dylan B. Millet[5], Kelley C. Wells[5], Xin Chen[5], Jared F. Brewer[1], Eric A. Ray[6,7], Róisín Commane[8], Glenn S. Diskin[9], and Steven C. Wofsy[10]

[1]School of Engineering and Applied Sciences, Harvard University, Cambridge, MA, USA, [2]Atmospheric Chemistry Observations & Modeling Laboratory, National Center for Atmospheric Research, Boulder, CO, USA, [3]Division of Geological and Planetary Sciences, California Institute of Technology, Pasadena, CA, USA, [4]Everactive, Inc., Charlottesville, VA, USA, [5]Department of Soil, Water, and Climate, University of Minnesota, St. Paul, MN, USA, [6]Earth System Research Laboratory, National Oceanic and Atmospheric Administration, Boulder, CO, USA, [7]Cooperative Institute for Research in Environmental Sciences, University of Colorado Boulder, Boulder, CO, USA, [8]Department of Earth and Environmental Sciences, Lamont-Doherty Earth Observatory, Columbia University, Palisades, NY, USA, [9]Langley Research Center, National Aeronautics and Space Administration, Hampton, VA, USA, [10]Department of Earth and Planetary Sciences, Harvard University, Cambridge, MA, USA

Key Points:

- Chemical production is the dominant source of background methanol in the remote troposphere
- The ocean is a net sink of atmospheric methanol and provides only a minor methanol source to the marine boundary layer
- The CH_3O_2 + OH reaction plays a key role in the atmospheric budgets not only of methanol but of many tropospheric radical species

Supporting Information:

- Supporting Information S1

Correspondence to:

K. Bates,
kelvin_bates@fas.harvard.edu

Citation:

Bates, K. H., Jacob, D. J., Wang, S., Hornbrook, R. S., Apel, E. C., Kim, M. J., et al. (2021). The global budget of atmospheric methanol: New constraints on secondary, oceanic, and terrestrial sources. *Journal of Geophysical Research: Atmospheres*, *126*, e2020JD033439. https://doi.org/10.1029/2020JD033439

Received 4 JUL 2020
Accepted 14 JAN 2021

Abstract Methanol is the second-most abundant organic gas in the remote atmosphere after methane, but its sources are poorly understood. Here, we report a global budget of methanol constrained by observations from the ATom aircraft campaign as implemented in the GEOS-Chem global atmospheric chemistry model. ATom observations under background marine conditions can be fit in the model with a surface ocean methanol concentration of 61 nM and a methanol yield of 13% from the newly implemented CH_3O_2 + OH reaction. While terrestrial biogenic emissions dominate the global atmospheric methanol budget, secondary production from CH_3O_2 + OH and CH_3O_2 + CH_3O_2 accounts for 29% of the total methanol source, and makes up the majority of methanol in the background marine atmosphere sampled by ATom. Net emission from the ocean is comparatively minor, particularly because of rapid deposition from the marine boundary layer. Aged anthropogenic and pyrogenic plumes sampled in ATom featured large methanol enhancements to constrain the corresponding sources. Methanol enhancements in pyrogenic plumes did not decay with age, implying in-plume secondary production. The atmospheric lifetime of methanol is only 5.3 days, reflecting losses of comparable magnitude from photooxidation and deposition. GEOS-Chem model results indicate that methanol photochemistry contributes 5%, 4%, and 1.5% of the tropospheric burdens of formaldehyde, CO, and ozone, respectively, with particularly pronounced effects in the tropical upper troposphere. The CH_3O_2 + OH reaction has substantial impacts on radical budgets throughout the troposphere and should be included in global atmospheric chemistry models.

Plain Language Summary Methanol is the most abundant nonmethane organic gas in the lower atmosphere, but the magnitudes of its sources and sinks remain uncertain. Here, we evaluate a global atmospheric chemistry model against recent observations of methanol in the remote atmosphere to better constrain the methanol budget. We show that, relative to past studies, the new data suggest a smaller atmospheric methanol source from the ocean and a larger source from gas-phase chemistry. Methanol emitted from the oceans plays a particularly small role in the atmosphere because it is quickly deposited back to the ocean surface. We incorporate these updates into the global model and evaluate their importance for atmospheric chemistry more broadly, showing that methanol directly and indirectly influences the abundances of many other tropospheric trace gases.

1. Introduction

Methanol is the most abundant nonmethane organic gas in the troposphere, where it influences the budgets of ozone and OH and is a precursor of formaldehyde and CO (Duncan et al., 2007; Tie et al., 2003; Wells

et al., 2014). The dominant source of methanol to the atmosphere is its primary emission from terrestrial plants, particularly during growth and decay stages (Ashworth et al., 2016; Galbally & Kirstine, 2002; MacDonald & Fall 1993; Warneke et al., 1999; Wohlfahrt et al., 2015). Additional sources include secondary production from the reactions of methylperoxy radicals (CH_3O_2) with CH_3O_2 and other organic peroxy radicals (Madronich & Calvert, 1990; Tyndall et al., 2001), as well as emissions from oceans (Heikes et al., 2002; Millet et al., 2008), biomass burning (e.g., Akagi et al., 2013; Hornbrook et al., 2011; Wentworth et al., 2018), and anthropogenic sources including solvent use, vehicular exhaust, and industrial processes (Legreid et al., 2007; Olivier et al., 1994; Velasco et al., 2009). Its sinks include reaction with OH (Sander et al., 2006), surface deposition (Karl et al., 2005, 2004; Mao et al., 2006; Talbot et al., 2005), and uptake by the ocean (Yang, Beale et al., 2014; Yang, Blomquist et al., 2014; Yang et al., 2013).

Due to its ubiquity, methanol has been the subject of many modeling studies providing estimates of its global budget in the atmosphere (Galbally & Kirstine, 2002; Heikes et al., 2002; Jacob et al., 2005; Khan et al., 2014; Millet et al., 2008; Singh et al., 2000; Stavrakou et al., 2011; von Kuhlmann et al., 2003). While these assessments tend to agree on the tropospheric burden of methanol (3–5 Tg), they exhibit large discrepancies in total sources and sinks (90–490 Tg a^{-1}), with even greater uncertainties for individual source terms. Comparisons with airborne observations (e.g., Jacob et al., 2005; Millet et al., 2008; Müller et al., 2016; Singh et al., 2000), ground-based measurements (e.g., Bader et al., 2014; Rinsland et al., 2009), and satellites (e.g., Dufour et al., 2006; Stavrakou et al., 2011; Wells et al., 2014, 2012) frequently show model biases in the seasonal and spatial variations of methanol and/or model underpredictions of observed methanol mixing ratios. Such underestimates are particularly acute in remote oceanic areas and exceed the uncertainties from methanol sinks, suggesting the need for additional secondary sources (Jacob et al., 2005; Müller et al., 2016; Stavrakou et al., 2011). Most recently, X. Chen et al. (2019) found that the global chemical transport model GEOS-Chem underestimated methanol mixing ratios by 60% in the boundary layer and 78% in the free troposphere over North America relative to observations from an ensemble of aircraft campaigns, accounting for nearly a quarter of the per-carbon simulated volatile organic compound (VOC) deficit. These disparities point to the ongoing need to better constrain the sources of tropospheric methanol.

An additional recently proposed source of methanol to the troposphere is the reaction of CH_3O_2 radicals with OH (Archibald et al., 2009; Fittschen et al., 2014), which is hypothesized to contribute substantially to the CH_3O_2 budget in the remote atmosphere where low NO leads to long peroxy radical lifetimes:

$$CH_3O_2^{\cdot} + OH \xrightarrow{k_{1a}} CH_3O^{\cdot} + HO_2 \quad (1a)$$

$$\xrightarrow{k_{1b}} CH_3OH + O_2 \quad (1b)$$

$$\xrightarrow{k_{1c}} CH_2OO^{\cdot\cdot} + H_2O \quad (1c)$$

$$\xrightarrow[M]{k_{1d}} CH_3OOOH \quad (1d)$$

The magnitude of this methanol source depends on the overall reaction rate ($k_1 = k_{1a} + k_{1b} + k_{1c} + k_{1d}$) and the fractional contribution of R1b to the overall reaction ($\phi_{1b} = k_{1b}/k_1$). Both numbers have been estimated in experimental and theoretical work but remain poorly constrained. Measurements of k_1 are in the range $(0.8–2.8) \times 10^{-10}$ cm^3 $molecule^{-1}$ s^{-1} (Assaf et al., 2016; Bossolasco et al., 2014; Yan et al., 2016), while observed and theoretical product yields suggest that R1a is the major pathway (≥80%), with ϕ_{1b} comprising 6%–9% and R1d making up the remainder (Assaf et al., 2017; Caravan et al., 2018; Müller et al., 2016; Yan & Krasnoperov, 2019). Modeling studies suggest that values of k_1 and ϕ_{1b} at the upper ends of these rang-

es could lead to substantial global methanol production (Ferracci et al., 2018; Khan et al., 2014); Müller et al. (2016) used the upper-limit uncertainty bound of $\phi_{1b} = 30\%$ to calculate a source strength of 115 Tg a^{-1}, comparable to primary terrestrial sources, which would resolve the model underestimate in remote areas. The methanol source from the CH_3O_2 + OH reaction could also be modulated by the effects on reaction rates and branching ratios of complexation between CH_3O_2 and water molecules in the atmosphere, or by subsequent production from the trioxide (CH_3OOOH) in reaction channel R1d (Butkovskaya et al., 2009; Caravan et al., 2018; Khan et al., 2015; Müller et al., 2016; Vaida, 2011). Crucially, the CH_3O_2 + OH reaction also competes with the methanol source from the CH_3O_2 + CH_3O_2 reaction; therefore, depending on the values of k_1 and ϕ_{1b}, including this reaction in global models could either decrease or increase secondary methanol production.

Among the other sources of methanol to the atmosphere, oceanic emissions remain highly uncertain. Early inventories of atmospheric methanol applied a fixed saturation ratio to the ocean surface (Jacob et al., 2005; Singh et al., 2003), effectively implying that the supply of methanol to seawater is controlled by uptake from the atmosphere. Later observations of sea-surface methanol indicated the presence of methanol sources and sinks within the surface ocean (Heikes et al., 2002; Williams et al., 2004), which has since been confirmed with the identification of methanol-producing phytoplankton (Mincer & Aicher, 2016) and methanol-consuming microbes (e.g., Giovannoni et al., 2008). Despite the presumed spatiotemporal heterogeneity of these biological controls on oceanic methanol, measured sea-surface concentrations have typically been high (100–200 nM) and homogeneous, which models invoked by applying two-way methanol exchange with a single fixed seawater concentration set to the average of past in situ measurements (e.g., Millet et al., 2008). However, recent studies have observed methanol concentrations an order of magnitude lower in the surface ocean (Yang, Beale et al., 2014; Yang, Blomquist et al., 2014; Yang et al., 2013) and with high interannual variability (Beale et al., 2015), suggesting the need to reevaluate the oceanic contribution to atmospheric methanol.

In this work, we reassess the global budget of methanol by updating the GEOS-Chem model to reflect the recent advances described above and compare simulations to measurements made during the NASA Atmospheric Tomography (ATom) Mission. We correlate model-measurement disparities in the most remote regions of the troposphere with simulated tagged methanol tracers to constrain the secondary and oceanic sources, and analyze observed enhancements of methanol mixing ratios in pyrogenic and anthropogenic plumes to evaluate the strength of those primary emissions. With these new source estimates, we present an updated global budget of tropospheric methanol. We further describe the contribution of methanol and the newly implemented CH_3O_2 + OH reaction to the budgets of formaldehyde, CO, ozone, and other trace tropospheric species.

2. Methods

2.1. GEOS-Chem

We simulate tropospheric methanol with GEOS-Chem, a three-dimensional global chemical transport model with detailed state-of-the-science atmospheric chemistry (http://geos-chem.org, last access: May 13, 2020). GEOS-Chem incorporates assimilated meteorological observations from the NASA Goddard Earth Observing System—Fast Processing (GEOS-FP) rdata product of the NASA Global Modeling and Assimilation Office. We use model version 11-02d including both tropospheric and stratospheric chemistry (Eastham et al., 2014) as well as updated halogen chemistry relevant to oxidant budgets in the remote and oceanic troposphere (Q. Chen et al., 2017; Sherwen, Evans et al., 2016; Sherwen, Schmidt et al., 2016). Methane mixing ratios are fixed in the model based on observations. In this work, we update the chemical mechanism with improved isoprene chemistry from Wennberg et al. (2018) using the implementation described in Bates and Jacob (2019). We also update the standard emissions inventories as described in the following section, including the addition of an oceanic alkane and alkene source following Paulot et al. (2011) and Millet et al. (2015). For comparisons with flight campaigns we sample the model at the times and locations of each observation, while for annual budget calculations we perform simulations from July 1, 2016 to June 30, 2017. All results described herein follow a model spin-up of at least 6 months and are performed at 2° × 2.5° horizontal resolution with 72 vertical levels.

We improve the diagnostic capability of GEOS-Chem by tagging methanol according to its source in order to separate the contributions from individual primary emission and secondary production sources. We add eight individual species: four representing primary biogenic, anthropogenic, pyrogenic, and oceanic methanol emissions, along with four representing secondary production of methanol from CH_3O_2 + CH_3O_2, CH_3O_2 + other organic peroxy radicals, glycolaldehyde photolysis, and the new CH_3O_2 + OH reaction. Each tagged methanol species has the same loss processes in the model as methanol itself; thus, the sum of the tagged tracers equals total methanol.

2.2. Model Sources and Sinks of Methanol

For biogenic methanol emissions from living plants, we use the Model of Emissions of Gases and Aerosols from Nature (MEGAN; Guenther et al., 2012) version 2.1, described in detail by Stavrakou et al. (2011). MEGAN calculates methanol emissions (E, mol m^2 s^{-1}) at each grid box and time step using the following formula:

$$E = \epsilon \times \gamma_{age} \times \gamma_{PT} \times \mathrm{LAI} \quad (2)$$

where ϵ represents a base emission factor dependent on plant type, γ_{age} is a scaling factor dependent on leaf age, γ_{PT} includes light- and temperature-dependent scaling, and LAI is the leaf area index. For methanol, ϵ is set to 6.94×10^{-9} mol m^2 s^{-1} for shrubs, crops, needle-leaf trees, and northern temperate and boreal broadleaf tree, and to 3.47×10^{-9} mol m^2 s^{-1} for grasses and all other broadleaf trees, based on 17 observational ecosystem studies (see citations in Guenther et al., 2006; Stavrakou et al., 2011). γ_{age} is based on Harley et al. (2007) and Karl et al. (2003) and is highest for young leaves, which produce large amounts of methanol from pectin demethylation during their growth (Fall & Benson, 1996; MacDonald & Fall, 1993). Finally, methanol emissions are highly light- and temperature dependent (Harley et al., 2007) and drop near zero at night due to stomatal control (Ashworth et al., 2016; Nemecek-Marshall et al., 1995). In MEGAN, this is incorporated into the γ_{PT} factor, which parameterizes 80% of methanol emissions as light-dependent and 20% as light-independent.

Methanol is also released from dead and decaying vegetation in various biotic and abiotic demethylation processes (Galbally & Kirstine, 2002; Warneke et al., 1999). We implement this source as in Jacob et al. (2005) and Millet et al. (2008), using an emission factor of 160 μg methanol emitted per kg dry plant mass applied to a map of heterotrophic respiration derived from the CASA 2 biosphere model (Potter et al., 1993; Randerson et al., 1997), which leads to a global methanol emission of 23 Tg a^{-1}.

When implemented in GEOS-Chem with GEOS-FP meteorology, MEGAN tends to underestimate biogenic VOC emissions (Bates & Jacob, 2019; Wells et al., 2014), so we scale MEGAN emissions up by 10% such that the primary biogenic source (from both living and dead vegetation) is equal to 100 Tg a^{-1}, as estimated by Stavrakou et al. (2011). While this source magnitude has also been corroborated by Millet et al. (2008) and Wells et al. (2014), multiple studies suggest that the spatiotemporal variability of methanol emissions is overly simplified by MEGAN. Rinsland et al. (2009) and Wells et al. (2014) both note a need for increased emissions from arid landscapes, and Wells et al. (2014) find that the seasonality of MEGAN emissions is biased. von Dahl et al. (2006) describe a large source from herbivory-induced plant stress that is currently absent from models. Wohlfahrt et al. (2015) review fluxes from land ecosystems and show that methanol emissions can differ substantially within plant functional types, for example, by up to a factor of 3 for various measurements of grasslands (Fukui & Doskey, 1998; Kirstine et al., 1998; Ruuskanen et al., 2011). However, the ATom observations are not suited to discern these details in the biogenic source, so we do not address these complexities here. Furthermore, despite the large regional and seasonal uncertainties in biogenic methanol emissions, our confidence in the global annual budget terms presented in Section 5 is elevated by the convergence of past inversion estimates (Wells et al., 2014).

Pyrogenic methanol emissions in GEOS-Chem are derived from the Global Fire Emissions Database version 4 (GFEDv4) (van der Werf et al., 2010). The calculation of gaseous emissions relies on burned area from Giglio et al. (2013) enhanced by the contribution of small fires as described in Randerson et al. (2012), with temporal scaling from Mu et al. (2011). Emission factors (g methanol emitted per kg dry material burned) for each of the six GFED4 burn types are based primarily on Akagi et al. (2011), ranging from 1.18 g kg^{-1}

for savannah fires to 8.46 g kg^{-1} for peat fires. In GEOS-Chem, this gives an annual methanol emission of 5.9 Tg a^{-1} in our base simulation used for initial comparisons and the regression analysis in Section 3. This is lower than previous global estimates, which range between 6 and 21 Tg a^{-1} (Andreae, 2019; Jacob et al., 2005; Millet et al., 2008; Wells et al., 2014), but gives an average molar ratio of pyrogenic methanol emissions to those of CO of 1.85% (mol mol^{-1}), in line with observed enhancement ratios of 0.9%–3.8% (Andreae & Merlet, 2001; de Gouw et al., 2006; Holzinger et al., 2005; Hornbrook et al., 2011; Lewis et al., 2013; Li et al., 2014; Simpson et al., 2011; Sinha et al., 2003, 2004; Warneke et al., 2009). As described in Section 4, we increase pyrogenic methanol emissions by a factor of 2.2 in the updated simulation for the global budgets in Section 5.

For anthropogenic methanol emissions, we use the MACCity emission data set (Lamarque et al., 2010) which specifically includes organic alcohols as a VOC class. We implement the RCP 8.5 forward-projected anthropogenic emissions to our period of interest and assume that methanol represents 50% of alcohol emissions by carbon mass (X. Chen et al., 2019), which gives a global methanol emission of 3.15 Tg a^{-1}, or 0.52% of CO emissions (mol mol^{-1}) in our base simulation. This is lower than total anthropogenic methanol emissions in most previous global model budgets, which are in the range 3–8 Tg a^{-1} (Jacob et al., 2005; Millet et al., 2008; Safieddine et al., 2017; Wells et al., 2014). As described in Section 4, we scale up anthropogenic methanol emissions by a factor of 2 in the updated simulation for the global budgets in Section 5.

The oceanic contribution to the atmospheric methanol budget is calculated locally as described by Fischer et al. (2012) for acetone in GEOS-Chem. Briefly, the parameterization is based on the two-film model of Liss and Slater (1974), by which the net flux (F, mol m^{-2} s^{-1}) out of the ocean can be calculated as the balance of ocean emission (E) and uptake (U) by the following equation:

$$F = E - U = -K_W \times (C_g \times H^{-1} - C_l) \quad (3)$$

where C_g and C_l represent the methanol concentrations in the air and water, respectively, H represents the dimensionless gas-over-liquid Henry's law equilibrium constant for methanol (2.02×10^{-4}, converted from 203 M atm^{-1} at 298 K, with a temperature dependence $d(ln(H))/d\,(1/T) = 5{,}600$ K, from Sander et al., 2006), and K_W represents the inverse of the total transfer resistance:

$$K_W^{-1} = k_l^{-1} + (H \times k_g)^{-1} \quad (4)$$

where k_l and k_g are the wind speed-dependent liquid- and gas-phase transfer velocities, calculated using the parameterizations from Nightingale et al. (2000) and Johnson (2010), respectively. Highly soluble gases such as methanol are limited primarily by air-side transfer, with the k_l term contributing only a few percent to the overall K_W (Yang et al., 2013). The dominant k_g term is the less-studied and more uncertain element of K_W, and studies in the laboratory and field frequently disagree on its parameterization (Johnson, 2010; Yang et al., 2013). We calculate the emission and uptake terms separately such that the gross outward methanol flux can be applied to the tagged oceanic methanol tracer, while the sink to the ocean can be applied to each of the tagged methanol tracers.

Oceanic methanol is presumed to be controlled primarily by in situ biological activity, supported by observations of rapid production and consumption of methanol by plankton and bacteria. The Prochlorococcus genus of phytoplankton alone was estimated to contribute 850–1700 Tg a^{-1} of methanol to the oceans, 10–40 times the contribution of deposition from the atmosphere (Mincer & Aicher, 2016). This source is offset by microbial uptake rates of up to 150 nM day^{-1} (Dixon et al., 2011b), giving methanol turnover times of <1 day. Methanol-consuming microbes have recently been observed and characterized in a wide variety of ocean environments (Arrieta et al., 2016; Deng et al., 2018; Dinasquet et al., 2018; Dixon et al., 2011a; Dixon & Nightingale, 2012; Dixon et al., 2013; Ramachandran & Walsh, 2015; Sargeant et al., 2016), including some obligate methylotrophs (Giovannoni et al., 2008), suggesting a critical role for methanol in the ocean microbiome. These various pathways of methanol production and destruction can be highly variable in both time and space. Production tends to peak only toward the end of the cell life cycle, and has been proposed to provide pulses of methanol associated with phytoplankton blooms (Mincer & Aicher, 2016). Dixon et al. (2013) and Sargeant et al. (2016) observed sharp geographic and seasonal contrasts in bacterial meth-

Table 1
Measurements of Methanol in the Surface Ocean

Concentration[a] (nM)	Location	Period	Reference
118.4 ± 48.2 (60–230)	Eq. Atl.	Oct–Nov 2002	Williams et al. (2004)
158.9 ± 33.1 (78–325)	NW. Pac.	Jul–Aug 2008	Kameyama et al. (2010)
139 ± 51 (48–361)	Atlantic[b]	Oct–Dec 2009	Beale et al. (2013) [c]
49 ± 15 (16–78)	coastal NE. Atl.	Feb 2011–Mar 2012	Beale et al. (2015)
29 (15–62)	Atlantic[b]	Oct–Nov 2012	Yang et al. (2013)
16.3 ± 5.5 (7–28)	N. Atl.	Oct–Nov 2013	Yang, Beale et al. (2014)
67 ± 35 (<21–226)	Southern Ocean	Feb–Apr 2020	Wohl et al. (2020)

[a]Reported values are means ± standard deviations; parentheses denote the complete range of observed values. [b]Full transect between 39°S and 49°N. [c]Also reported in Beale et al. (2011) and Read et al. (2012).

anol consumption rates, with different metabolic pathways (used as an energy source vs. for cell growth) dominating in different regions.

Despite the presumed spatiotemporal heterogeneity of oceanic methanol sources and sinks, observations of sea-surface methanol (summarized in Table 1) exhibit little correlation with biological activity and no obvious patterns of spatial and temporal variability. Instead, there is a distinct divergence between early observations (pre-2010), which measured mean concentrations of 118–159 nM, and more recent observations of <70 nM, including many in similar locations and seasons to the high prior observations. Past global inventories have typically used a fixed surface seawater concentration of 118 nM, the mean concentration observed by Williams et al. (2004), and found that the ocean provides a gross methanol source of 43–85 Tg a^{-1} offset by a gross sink of 48–101 Tg a^{-1}, balancing to a net sink of 5–16 Tg a^{-1} (Millet et al., 2008; Stavrakou et al., 2011; Wells et al., 2014, 2012). Wells et al. (2014) performed sensitivity simulations in which the seawater concentration was varied by ±41%, which caused the net ocean sink to vary from 0 to 15 Tg a^{-1}.

Here, to test the potential impact of a lower oceanic methanol concentration in line with recent measurements, we set a fixed seawater concentration of 31.4 nM (the mean of the three most recent Atlantic observations in Table 1) in our base simulation, which provides a gross source term of 13 Tg a^{-1} balanced by a computed gross sink term of 30 Tg a^{-1}, for a net sink of 17 Tg a^{-1}. We adjust the seawater concentration for our updated simulation as described in Section 3 and find that a fixed seawater concentration of 61 nM provides the best fit to ATom observations, which yields gross source, gross sink, and net sink terms of 24, 38, and 14 Tg a^{-1}.

Among the sources of secondary methanol in the standard GEOS-Chem mechanism, the $CH_3O_2 + CH_3O_2$ reaction dominates, producing 45 Tg a^{-1} of methanol. The reaction proceeds by two competing pathways:

$$CH_3O_2^{\cdot} + CH_3O_2^{\cdot} \xrightarrow{k_{5a}} CH_3OH + CH_2O + O_2 \quad (5a)$$

$$\xrightarrow{k_{5b}} 2CH_3O^{\cdot} + O_2 \quad (5b)$$

GEOS-Chem uses an overall rate coefficient $k_5 = k_{5a} + k_{5b}$ of $9.5 \times 10^{-14} \times e^{390/T}$ (Sander et al., 2006) and a temperature-dependent branching ratio of $k_{5b}/k_{5a} = 26.2 \times e^{-1130/T}$ (Tyndall et al., 2001). The methyl peroxy radical can also react with other peroxy radicals (represented as RO_2) to produce methanol:

$$CH_3O_2^{\cdot} + RO_2^{\cdot} \xrightarrow{k_{6a}} CH_3OH + R_H{=}O + O_2 \quad (6a)$$

$$\xrightarrow{k_{6b}} CH_3O^{\cdot} + RO^{\cdot} + O_2 \quad (6b)$$

$$\xrightarrow{k_{6c}} CH_2O + ROH + O_2 \quad (6c)$$

In GEOS-Chem, the branching ratio to methanol production $\left(k_{6a} / (k_{6a} + k_{6b} + k_{6c})\right.$ ranges from 20% to 50% for primary and secondary peroxy radicals, and is set to zero for tertiary and acyl peroxy radicals without available hydrogen atoms (Orlando & Tyndall, 2012). The photolysis of glycolaldehyde also produces methanol, with a yield of 10% in GEOS-Chem (Magneron et al., 2005). Together, the contributions of R6a and glycolaldehyde photolysis add only 3.2 Tg a^{-1} of methanol to the global budget in the standard GEOS-Chem mechanism.

Here, we update the GEOS-Chem chemical mechanism by adding the reaction of CH_3O_2 with OH radicals (R1), as described in the introduction. In the base simulation, we set the reaction rate (k_1) to the median observed value of 1.6×10^{-10} cm^3 $molecule^{-1}$ s^{-1} (Assaf et al., 2016), and set the methanol yield (ϕ_{1b}) to 7%, the central estimate of both Müller et al. (2016) and Caravan et al. (2018), with the remainder forming formaldehyde + $2HO_2$ by pathway R1a (the alkoxy intermediate shown in R1a is assumed to react promptly with O_2). Consistent with experimental and theoretical results, we do not include pressure or temperature dependence in either k_1 or ϕ_{1b}. We then adjust the methanol yield from R1 based on ATom observations, as described in Section 3 along with additional sensitivity studies of different rates and product yields. As implemented in the base simulations, R1 provides a methanol source of 18 Tg a^{-1}. However, because it competes as a sink for CH_3O_2 radicals, the inclusion of R1 in GEOS-Chem decreases the methanol sources from R5 and R6 by 21 Tg a^{-1} and 0.3 Tg a^{-1} respectively, thus diminishing the total secondary production of methanol in the model, consistent with the results of Caravan et al. (2018). In our updated model, we find that a yield ϕ_{1b} of 13% provides the optimal fit to ATom observations (see Section 3), which gives a methanol source of 33 Tg a^{-1}.

In addition to ocean uptake described above, methanol loss processes in GEOS-Chem include reaction with OH and the chlorine radical as well as dry and wet deposition to land surfaces. The reaction of methanol with OH proceeds with a rate coefficient of $k = 2.9 \times 10^{-12} \times e^{-345/T}$, resulting in a globally averaged lifetime of methanol against reaction with OH of 9 days. Contradictory studies suggest that the reaction of OH with methanol may or may not be accelerated in the presence of water vapor (Chao et al., 2019; Jara-Toro et al., 2017); absent any conclusive evidence, we do not include this catalysis in our simulations. Dry deposition employs the standard GEOS-Chem resistance-in-series parameterization (Y. Wang et al., 1998), updated to account for reactive uptake by vegetation (Karl et al., 2010), resulting in a lifetime of methanol against dry deposition to land surfaces of 27 days, comparable to the 29 days globally averaged lifetime against ocean uptake in the updated model. Wet deposition and oxidation by aqueous OH in cloud water, both unchanged from previous GEOS-Chem analyses (Jacob et al., 2005; Wells et al., 2014), and the reaction of methanol with Cl, newly implemented here with a rate constant of $k_{Cl} = 5.5 \times 10^{-11}$ (Atkinson et al., 2006), are minor loss pathways, with associated lifetimes of 98, 1,100, and 650 days, respectively. Sensitivity analyses by Wells et al. (2014) suggest that perturbing the methanol sinks within their uncertainty ranges does not appreciably alter the global methanol budget or source estimates in GEOS-Chem; we therefore do not test changes to methanol loss processes, aside from ocean uptake, in our optimization.

2.3. Observations from the NASA ATom Campaign

Observations of methanol and other trace gases were conducted as part of the NASA ATom field mission. The ATom campaign included four individual deployments: July–August 2016, January–February 2017, September–October 2017, and April–May 2018. Each deployment consisted of a month-long series of flights starting and ending in Palmdale, California, during which the NASA DC-8 aircraft flew the full north-south lengths of the Pacific and Atlantic Oceans, repeatedly ascending and descending between altitudes of 200 m and 10–12 km to profile the troposphere.

A comprehensive suite of instruments aboard the DC-8 measured numerous trace gases, aerosol properties, and other atmospheric quantities. Previous work comparing these measurements to GEOS-Chem and other models have revealed the need for novel or increased oceanic sources of many VOCs, including acetalde-

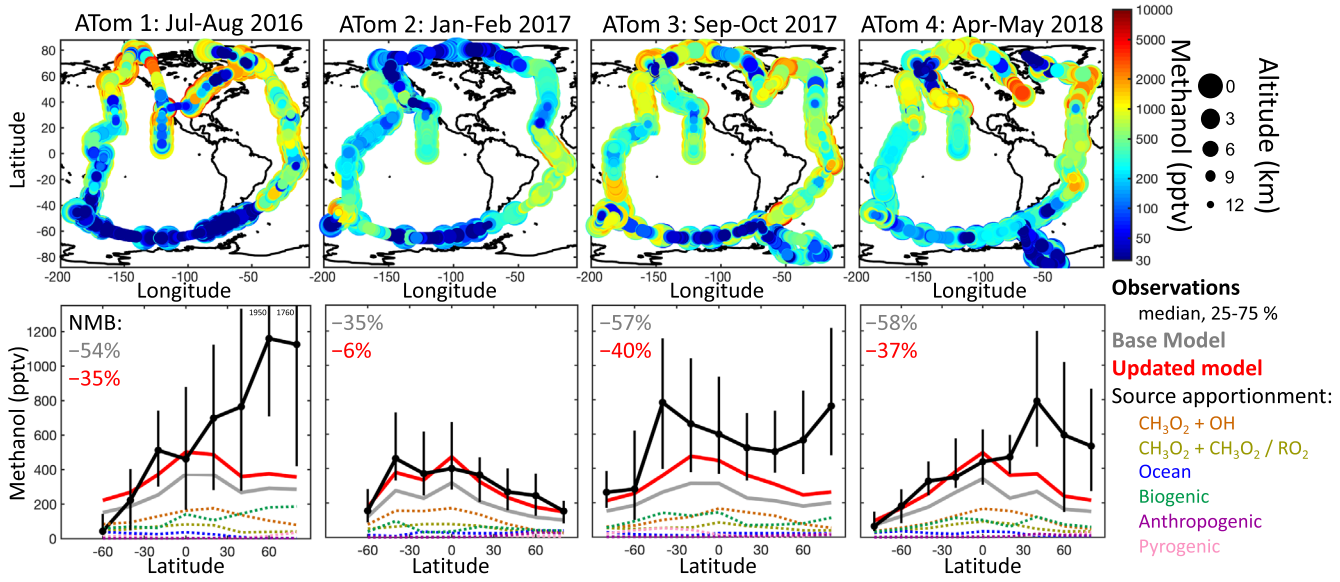

Figure 1. Methanol concentration during the Atmospheric Tomography (ATom) mission. Top panels show measured methanol along the ATom flight tracks; point colors correspond to the methanol mixing ratio, while point size corresponds to altitude. Bottom panels show simulated and measured methanol binned by 20° latitude intervals for each ATom mission. Measurement medians along with 25–75 percentile ranges are shown in black, while medians from the base and updated models are shown in gray and red, respectively, and source contributions from the updated model are shown in colored dashed lines.

hyde (Travis et al., 2020; S. Wang et al., 2019), acetone (S. Wang et al., 2020), methyl ethyl ketone (Brewer et al., 2020), and small alkyl nitrates (Fisher et al., 2018). Even with these updated sources, acetaldehyde remains underestimated in both GEOS-Chem and CAM-chem throughout the troposphere, suggesting the need for an unknown VOC precursor (S. Wang et al., 2019). Such a precursor would also contribute to OH reactivity in the marine boundary layer, for which both Thames et al. (2020) and Travis et al. (2020) show a persistent negative bias. Despite this, Travis et al. (2020) found that GEOS-Chem successfully simulated tropospheric OH and its sources to within measurement uncertainty, and that simulated NO_y was also satisfactory aside from a high bias in wintertime HNO_3 in the northern hemisphere. Because the source of CH_3O_2 is governed primarily by OH and methane (fixed to observations in GEOS-Chem), this provides confidence that remote CH_3O_2 production is unbiased in the model, and thus that the CH_3O_2 + OH reaction is well represented.

Methanol and other organic gases discussed here, including hydrogen cyanide (HCN) and acetonitrile (CH_3CN), were measured with the NCAR Trace Organic Gas Analyzer (TOGA), details of which can be found in previous publications (Apel et al., 2010, 2003, 2015; Hornbrook et al., 2011). TOGA combines a cryogenic preconcentrator, a gas chromatograph (Restek MXT 624 8-m column, 0.18 mm inner diameter), and an Agilent 5973N mass spectrometer to measure mixing ratios of numerous VOCs. TOGA has a total sample throughput time of 2 minutes, which enabled 11,517 individual observations of methanol (and other VOCs) over the course of the four ATom deployments. The precise inlet configuration and other details of the TOGA setup in ATom can be found in S. Wang et al. (2019). Precision and accuracy for the detection of methanol by TOGA were estimated at 10 pptv and 30%, respectively. Inorganic gases used in the present analysis include CO measured by quantum cascade laser spectrometer (QCLS) and water vapor measured with a diode laser hygrometer (Diskin et al., 2002; McManus et al., 2005), both averaged to the same observation frequency as the TOGA measurements. For periods when the QCLS was calibrating, CO measurements with a Picarro Analyzer were used instead, corrected for difference from the QCLS with a low-pass filter.

3. Constraints on Secondary and Oceanic Methanol Sources

Figures 1 and S1 show measured methanol mixing ratios along the ATom flight tracks. ATom observations, as with previous campaigns, exhibit a persistent high methanol background of several hundred pptv throughout the troposphere. The highest mixing ratios (several ppbv) are encountered over North America

in summer, when biogenic emissions peak (Wells et al., 2012), and in biomass burning plumes frequently observed during Atlantic transects. The lowest levels (tens of pptv) are found in the stratosphere and in the high latitudes during winter months. There is pronounced seasonal variability at high northern latitudes and southern mid-latitudes (high in spring-summer, low in winter), but variability elsewhere is driven primarily by the interception of continental plumes.

Figures 1–3 show comparisons between GEOS-Chem simulations and ATom observations as functions of latitude, altitude, and region. For a complete breakdown by season as well, see Figures S2–S4. While the model generally captures the features of the methanol altitude profiles and seasonal cycles both globally and regionally, the base model (in gray) exhibits a substantial negative bias, underestimating methanol globally by over 50% (normalized mean bias). The model bias is largest in the Arctic, where it exceeds 70%, and in the northern mid-latitudes, except during winter; it is smallest in equatorial regions and over the Southern Ocean. Only over the Southern Ocean in austral winter does the base model overestimate the tropospheric methanol column. Averaged across seasons, however, the negative model bias exceeds 30% everywhere, suggesting a ubiquitously underestimated methanol source throughout the troposphere.

On a global scale, the negative model bias is strongly correlated with HCN, benzene, and CO (see Figure S5), suggesting that pyrogenic, anthropogenic, and potentially biogenic sources are underestimated. However, these biases from terrestrial sources might be caused by a number of factors that are difficult to disentangle because ATom provided only limited and indirect information on source regions. Here, we seek to isolate the observations remote from continental influence in order to focus on the highly uncertain CH_3O_2 + OH and oceanic contributions to the budget, which will enable us to fit the measurement-model difference with the following equation:

$$CH_3OH_{TOGA,i} - CH_3OH_{base,i} = \alpha \times CH_3OH_{OH,i} + \beta \times CH_3OH_{ocean,i} + \epsilon_i \quad (7)$$

where $CH_3OH_{TOGA,i}$ represents the methanol mixing ratio measured by TOGA at point i, $CH_3OH_{base,i}$ represents the base simulated methanol at that point, and $CH_3OH_{OH,i}$ and $CH_3OH_{ocean,i}$ represent the tagged methanol from the CH_3O_2 + OH and oceanic sources, respectively. We then find the values of the coefficients α and β, constrained to stay above −1 to avoid negative source terms, that minimize the sum of the squared errors ϵ_i; the resulting coefficients represent the scaling factors that need to be applied to the CH_3O_2 + OH and oceanic sources in order to minimize the model underestimate. The CH_3O_2 + OH and oceanic methanol sources exhibit little collinearity (variance inflation factor = 1.08). Key assumptions and uncertainties inherent to this approach are discussed at the end of the section.

To isolate remote tropospheric points, we exclude from the present analysis any TOGA observations over land, stratospheric points (those with measured water vapor below 15 ppmv), as well as points for which benzene, CO, and HCN exceed certain background thresholds. We vary these thresholds to find a combination that includes the maximum number of observations while minimizing the correlations with CO, HCN, and benzene (determined by separately adding terms for each species to the fit in Equation 7, for example, $\delta \times CO_{obs,i}$, and finding the corresponding coefficient δ indistinguishable from or less than zero at the 95% confidence level). The resulting threshold values are 3 ppbv for benzene, 200 pptv for HCN, and a latitude-dependent CO background rising linearly from 60 ppbv at and below 45°S to 120 ppbv at and above 45°N. This results in 1,861 remote TOGA samples to use in the fit in Equation 7; the locations of these remote samples are shown in Figure S6. The coefficient estimates described below are insensitive to moderate changes in the precise choice of background threshold; for example, increasing any of the threshold mixing ratio values by 20%, replacing the HCN threshold with CH_3CN, or replacing the latitude-dependent CO threshold with a fixed threshold of 100 ppbv all result in coefficient estimates that are not statistically different from those we report here.

After isolating the remote points, we find that the best fit in Equation 7 gives coefficients of $\alpha = 0.88 \pm 0.06$ and $\beta = 0.94 \pm 0.09$ (reported error bounds are standard deviation estimates using the bootstrapping method). Applying these coefficients to the CH_3O_2 + OH and oceanic methanol sources respectively removes the negative model bias for remote points, as shown in Figure 2, and reduces the absolute mean error (AME) and root mean squared error (RMSE) by 25% (see Figure S7). Applying these coefficients to the full ATom data set reduces the overall model bias from −56% to −31%, with the strongest effects in the

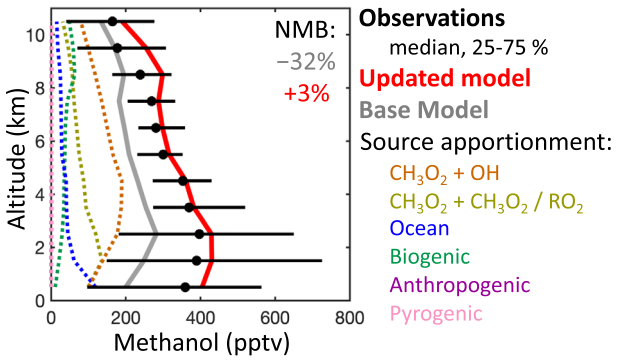

Figure 2. Altitude profiles of measured and simulated remote methanol mixing ratios during the Atmospheric Tomography (ATom) mission. Measurement medians along with 25–75 percentile ranges are shown in black, while medians from the base and updated models are shown in gray and red respectively, and source contributions from the updated model are shown in colored dashed lines, all binned by 1 km altitude intervals.

equatorial regions and over the Southern Ocean (Figures 3d, 3f, and 3h). Averaged across seasons, the model bias is eliminated over the equatorial Pacific, the region with the fewest intersected continental plumes and the highest relative contribution from secondarily produced methanol. However, methanol remains underestimated by the model in parts of the troposphere influenced by continental sources, where a greater number of measurements were excluded from the remote source analysis due to elevated CO, HCN, and benzene. This underestimate is most pronounced in the northern mid- and high latitudes (Figures 3a–3c), except during winter, suggesting that Northern Hemispheric terrestrial methanol sources remain underestimated in the updated model. The contribution of model biases in anthropogenic and pyrogenic methanol emissions to this underestimate will be addressed in Section 4. While a lack of long-lived biogenic tracers precludes a quantitative analysis of model bias in biogenic methanol emissions with the ATom data, the simulated source contribution profiles (Figures S2 and S3) and seasonality of the bias suggest that Northern Hemispheric biogenic emissions may be underestimated with MEGAN in GEOS-Chem, as previously found for the United States and Western Europe by Wells et al. (2014).

The values of the coefficients α and β imply a branching ratio of methanol formation from the CH_3O_2 + OH reaction of $\phi_{1b} = 13.2 \pm 0.4\%$ and a uniform oceanic surface methanol concentration of 61 ± 3 nM. While a 13% methanol yield through Reaction R1b is larger than the most recent experimental estimates (Caravan et al., 2018), it remains within the uncertainty bounds of measured total methanol formation from Reaction R1, including possible contributions from an increased rate or from secondary formation via the trioxide (R1d). Indeed, the overall methanol yield from Reaction R1 estimated by Müller et al. (2016), including via R1d, totals 11.5%. We test these possibilities with two sensitivity simulations, identical to the base simulation but with (a) a faster k_1 rate (2.8×10^{-10} cm^3 molecule^{-1} s^{-1}), causing decreased methanol production from CH_3O_2 + CH_3O_2 but increased production from CH_3O_2 + OH, and (b) the addition of channel d to Reaction R1, forming the trioxide CH_3OOOH, which reacts as in Müller et al. (2016) to form additional methanol, such that the total methanol yield is 13%. Refitting Equation 7 with the output of these simulations results in a worse fit for case (a) (lower R^2, higher AME and RMSE) and an indistinguishable fit for case (b). Thus, we cannot determine from our simulations whether methanol production from CH_3O_2 + OH is prompt or proceeds through a trioxide intermediate, but we achieve the best fit to methanol observations with an overall yield of 13%.

Our inferred ocean concentration of 61 nM is within the bounds of previous measurements, and closer to the recent low values observed by Yang et al. (2013), Yang, Blomquist et al. (2014), and Beale et al. (2015). While it is nearly 50% lower than the value of 118 nM used in previous global models, which was prescribed on the basis of early measurements by Williams et al. (2004), the resulting net global flux of methanol (14 Tg a^{-1} from the atmosphere to the ocean), shown in Figure 4, is comparable in magnitude and spatial variability to previous budgets (e.g., Figure 3 in Millet et al., 2008). Our oceanic methanol uptake is equivalent to a mean deposition velocity of 0.67 cm s^{-1} across the ocean surface; while this is higher than past estimates inferred from atmospheric methanol profiles and trends (Carpenter et al., 2004; Singh et al., 2003), it compares well with more recent estimates from eddy covariance flux measurements, which averaged 0.68 cm s^{-1} across the Atlantic Ocean (Yang et al., 2013).

Our constraint on the oceanic contribution to atmospheric methanol is predominantly on the net flux, while the absolute seawater methanol concentration we derive from our fitting is highly sensitive to the air-sea exchange parameterization scheme. We test this by performing a sensitivity simulation in which we replace the methanol uptake term in Equation 3 with the generic dry deposition scheme from GEOS-Chem and refit Equation 7 with the resulting output. While deposition to the ocean decreases by a factor of 2, we find that the coefficient β drops in tandem to give a comparable net oceanic flux and quality of fit. Furthermore, our inferred ocean fluxes across the low-to-mid-latitude Atlantic of 3–10 μmol m^{-2} day^{-1} (Figure 4a) are comparable to the only in situ flux observations available, which measured mean values of

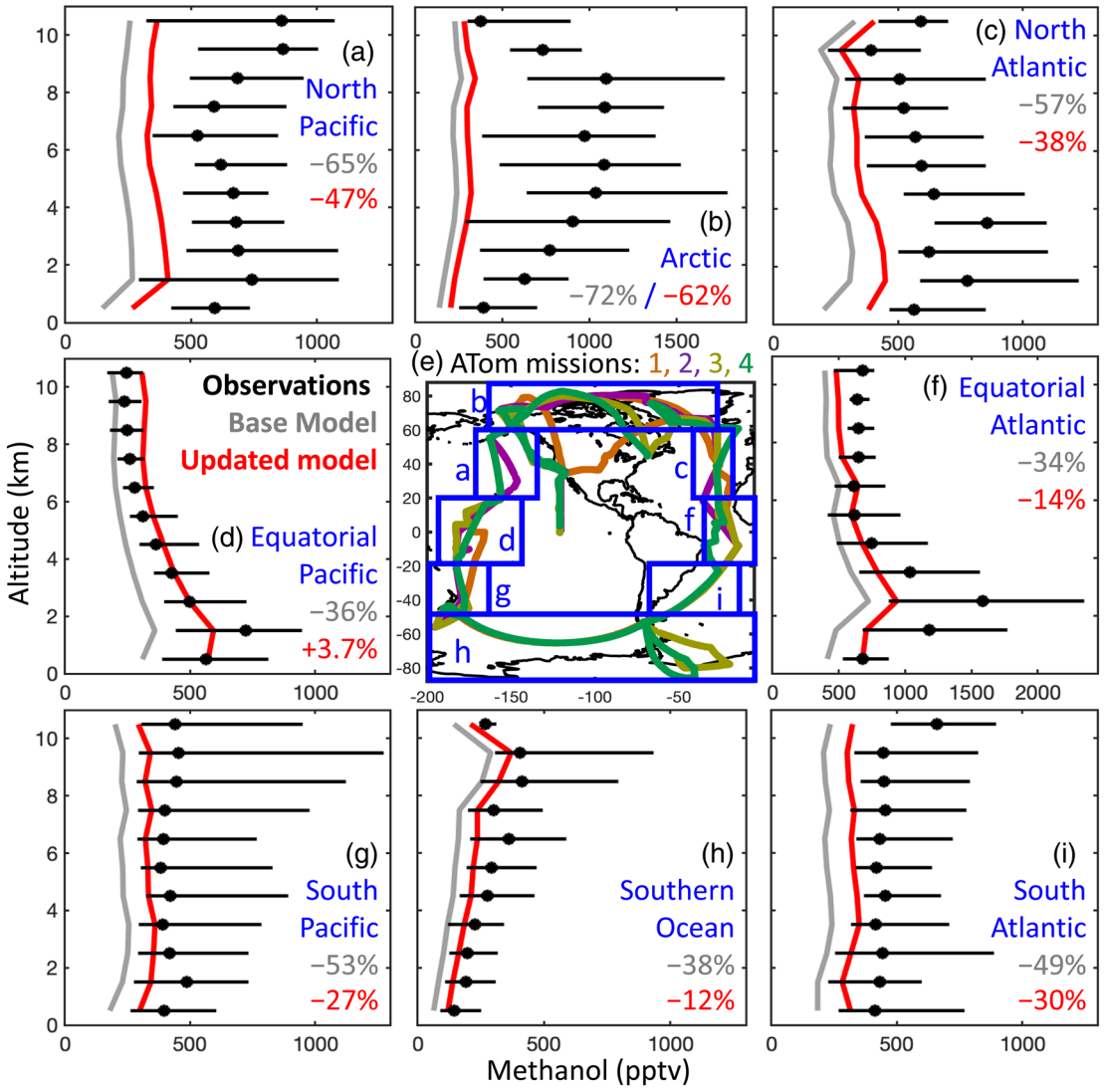

Figure 3. Regional altitude profiles of measured and simulated methanol mixing ratios during the Atmospheric Tomography (ATom) mission. Measurement medians along with 25–75 percentile ranges are shown in black, while medians from the base and updated models are shown in gray and red, respectively. Regional boundaries and ATom flight tracks are shown on the map at center (e). Altitude scales are identical between panels, but methanol scales differ.

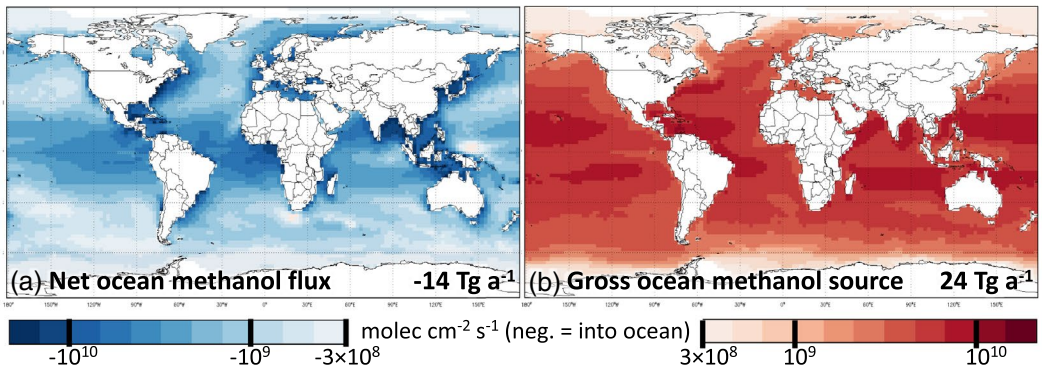

Figure 4. Simulated ocean-atmosphere methanol exchange. The left panel shows the annual average net flux of methanol from the ocean to the atmosphere, while the right panel shows the annual average gross oceanic methanol emissions, both in the updated simulation. Negative fluxes in the left panel indicate net uptake.

8.0 and 12.5 μmol m^{-2} day^{-1} in the Southern and Northern Hemispheric Atlantic, respectively (Yang, Beale et al., 2014; Yang, Blomquist et al., 2014) and 15 μmol m^{-2} day^{-1} in the Northwest Atlantic (Yang, Blomquist et al., 2014). These sensitivity tests and comparisons provide confidence in our inferred values of net methanol flux, but future work incorporating surface and ocean measurements will be needed to better constrain gross fluxes and to quantify their relationship with sea-surface methanol concentrations.

The formulation of Equation 7 prescribes a uniform correction factor for the concentration of methanol in the surface ocean, but the wide range of surface ocean methanol concentrations measured in situ suggest that sea-surface methanol is nonuniform. In particular, recent measurements of sea-surface methanol by Wohl et al. (2020) show high variability and correlation with biogeochemical parameters in the Southern Ocean, suggesting that local-to-regional surface methanol may vary predictably in space and time. To test this possibility, we replace the single β coefficient in Equation 7 with a vector $\vec{\beta}$ which applies a different coefficient to oceanic methanol in each ocean basin and season. We test this by splitting the ocean source term by ATom mission and by the regions shown in Figure 3 (excluding the Arctic, which lacks sufficient remote points) and refitting Equation 7, constraining all coefficients to be greater than −1. This gives $\alpha = 0.85 \pm 0.04$ (not significantly different from the fixed-ocean fit) and surface seawater methanol concentrations between 0 and 300 nM. While these values fall within measured ranges, the overall fit between the model and observations is not substantially improved, and few of the individual oceanic coefficients are sufficiently constrained to be significantly different from the fixed value. Furthermore, in some seasons and regions with few observations that qualify as remote, the highly uncertain local best fit β results in high (∼300 nM) oceanic methanol and a near-surface atmospheric methanol gradient inconsistent with observations. For completeness, we show the variable-ocean profiles as dashed lines in Figures S2 and S3 and provide the inferred concentrations in Table S1, but we continue to use the fixed-ocean simulations for the rest of the present analysis. Further research incorporating surface measurements will be needed to diagnose seasonal and regional variability in surface ocean methanol concentrations.

Even allowing for a variable ocean concentration, the linear fitting method used here includes a number of inherent assumptions: first, that the total simulated methanol will respond linearly to perturbations in the sources; second, that the CH_3O_2 + OH and oceanic terms are parameterized correctly, requiring only linear modifications; and third, that the CH_3O_2 + OH and oceanic terms are the only sources responsible for the model bias. We see little reason to assume the first assumption does not hold, as minor modifications to the methanol budget should not cause nonlinear behavior such as a strong reduction in OH (see Section 5.1). We have already described sensitivity studies designed to test the second assumption (e.g., varying the k_1 rate, implementing a trioxide intermediate in the CH_3O_2 + OH reaction, and testing ocean deposition schemes), from which we conclude that, while plausible, these changes to the source parameterizations would not substantially change our inferences about the contributions of these sources to the methanol budget.

We test the third assumption—that the CH_3O_2 + OH and oceanic terms are the only sources that contribute to the model bias in the remote troposphere—in two ways. First, we add terms to Equation 7 for each of the six other tagged tracers from the simulation and refit the model-measurement difference for remote points. Each of the terms result in coefficients indistinguishable from or equal to zero. Second, we perform a sensitivity simulation in which we increase the rate of the reaction between OH and methanol by 5%, to test whether perturbations to the methanol sink might influence the results. Refitting Equation 7 using the results of this simulation, with or without the additional tagged tracers, results in an indistinguishable fit with a slightly smaller coefficient α (within uncertainty). Between these tests and eliminating the correlations of the model bias with CO, HCN, and benzene, we believe we have isolated the parts of the atmosphere where only the CH_3O_2 + OH and oceanic sources contribute to the bias; however, we cannot rule out the possibility that additional sources not considered here, such as secondary production from another methyl peroxy reaction pathway or from additional ocean-derived VOCs, may play a role. This would cause our coefficients α and β to be overestimated. However, our updated simulation would still have the correct approximate total source strength in the remote troposphere for the purposes of global budget estimates (Section 5); the source would just be erroneously attributed to the CH_3O_2 + OH and oceanic terms instead of any unidentified source we exclude.

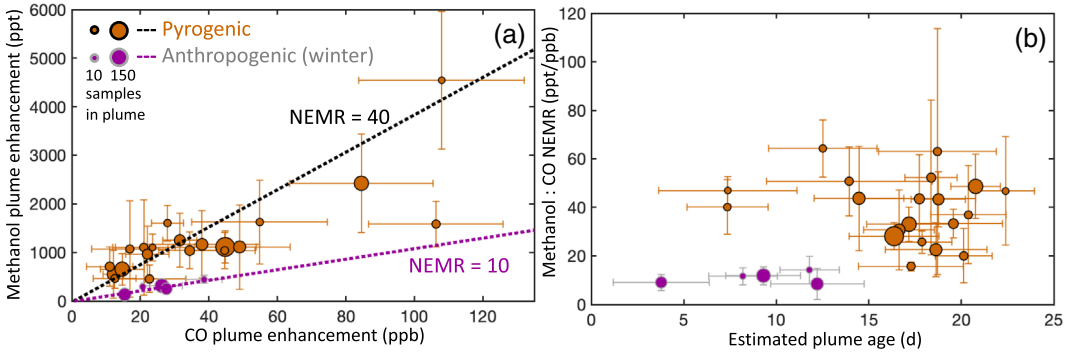

Figure 5. Pyrogenic and anthropogenic plumes in the Atmospheric Tomography mission. (a) Methanol and CO enhancements above background in each sampled plume; points are sized by the number of observations, and lines represent weighted mean methanol:CO normalized excess mixing ratios (NEMRs) for all pyrogenic plumes and for wintertime anthropogenic plumes. (b) Methanol:CO NEMRs and estimated ages (from back-trajectories; see Supporting Information) of each sampled plume. Error bars represent the propagated error from the standard deviations of methanol and CO observations and estimated plume age in each plume and background sample, and do not include the instrumental uncertainty or uncertainty in individual plume age estimates.

4. Plume-Based Constraints on Terrestrial Sources

Despite its focus on the remote atmosphere, the ATom mission sampled a number of strong terrestrial plumes. Our ability to diagnose the model-measurement disparity in these plumes from the regression analysis used in Section 3 is limited for at least two reasons. First, global-scale plume transport in Eulerian models is hampered by fast numerical diffusion in sheared or divergent flows (Eastham & Jacob, 2017; Zhuang et al., 2018). Second, the model bias in terrestrial source strength is likely highly heterogeneous; using a fitting procedure as in Equation 7 to constrain terrestrial sources would fail to account for this heterogeneity, as it assumes the spatiotemporal pattern of methanol emissions is correct and only requires linear scaling.

Instead, we examine the potential for the ATom data set to provide constraints on pyrogenic and anthropogenic methanol emissions by isolating individual plumes and comparing their elevated levels of methanol to previous measurements and to the emission ratios used in GEOS-Chem. Our metric for comparison is the normalized excess mixing ratio (NEMR), calculated as:

$$NEMR = 1000 \times \frac{\Delta[CH_3OH]}{\Delta[CO]} = \frac{[CH_3OH]_{plume} - [CH_3OH]_{background}}{[CO]_{plume} - [CO]_{background}} \quad (8)$$

We identify plumes as in Hornbrook et al. (2011), isolating periods of sharply delineated increases in CO and methanol, and selecting the closest available unelevated samples at a similar altitude as a background. Details for individual plumes are reported in Tables S2 and S3. We categorize plumes as pyrogenic if they are accompanied by elevated HCN and CH_3CN ($NEMR_{CH_3CN:CO}$ >1.5), and anthropogenic if not. Unfortunately, a lack of exclusively biogenic tracers in continental plumes observed during ATom precludes quantification of biogenic methanol emissions. The selected backgrounds may differ from the continental boundary layer backgrounds of methanol and CO, adding large uncertainty to the calculated NEMR (Mauzerall et al., 1998). In addition, pyrogenic and anthropogenic sources of methanol and CO are likely to coincide with biogenic emissions, which may then be misattributed. To minimize this interference, we isolate only the wintertime anthropogenic plumes for further analysis; we do not find a significant seasonal difference in NEMR for pyrogenic plumes, which are generally more distinct (higher mixing ratio enhancements above background) than anthropogenic plumes. We calculate the methanol NEMR individually for each of the 20 identified pyrogenic and 6 wintertime anthropogenic plumes, then use as our central estimate the mean NEMR across plumes, weighted both by the error-propagated standard deviation in the plume NEMR and the number of points per plume.

Table 2
Global Budget of Atmospheric Methanol

	Previous estimates[a]	This work[b]
All sources (Tg a^{-1})	214 (105–287)	205
Terrestrial biogenic[c]	110 (95–230)	101
Biogenic growth	100 (75–280)	78
Biogenic decay	20 (13–23)	23
Anthropogenic	4.5 (1–9.3)	6.3
Pyrogenic	11 (4.3–13)	13
Oceanic[d]	43 (30–85)	24
Secondary production[c]	37 (18–48)	60
$CH_3O_2 + CH_3O_2$	31 (15–48)	24
$CH_3O_2 + OH$[e]	18 (8–44)	33
Other reactions[e]	3.0	3.0
All sinks (Tg a^{-1})	214 (105–299)	205
Reaction with OH	104 (66–218)	114
Reaction with Cl[f]	1.4	1.7
Ocean uptake[d]	61 (10–101)	38
Wet deposition	11 (2.7–13)	11
Dry deposition to land	34 (24–70)	41
In-cloud oxidation	<1 (0–10)	<1
Lifetime (days)	6.6 (4.7–12)	5.3
Burden (Tg)	3.4 (2.9–5)	3.0

[a]Median and range of central estimates from the following previous global budget analyses: Singh et al. (2000), Galbally and Kirstine (2002), Heikes et al. (2002), von Kuhlmann et al. (2003), Tie et al. (2003), Jacob et al. (2005), Millet et al. (2008), Stavrakou et al. (2011), Wells et al. (2014), Khan et al. (2014), and Müller et al. (2016). [b]Global GEOS-Chem budget from our updated simulation. [c]Subcategories do not sum to category totals because they only include those studies that specify the biogenic and secondary pathways. [d]Including only those studies that report gross oceanic emissions and uptake, rather than net values. [e]Only Müller et al. (2016) and Khan et al. (2014) included the $CH_3O_2 + OH$ source, and only von Kuhlmann et al. (2003) quantified the contributions of other secondary pathways (including $CH_3O_2 + RO_2$ and glycolaldehyde photolysis). [f]Only Müller et al. (2016) separately accounted for this sink.

Figure 5a shows the CO and methanol enhancements of individual plumes along with the weighted mean NEMRs for pyrogenic and wintertime anthropogenic plumes, for which we find values of 39.8 ± 13 ppt ppb^{-1} and 10.4 ± 2.1 ppt ppb^{-1}, respectively. Our observed pyrogenic NEMR is higher than most previous measurements (10–31; Hornbrook et al., 2011; Lewis et al., 2013; Li et al., 2014, and references therein), but not implausible; Holzinger et al. (2005) measured a methanol:CO NEMR of 38 ppt ppb^{-1} in aged biomass burning plumes over the Eastern Mediterranean. It suggests that the GFED-derived methanol:CO emission ratio of 1.85% in GEOS-Chem should be increased by a factor of 2.2, which brings the total pyrogenic methanol emissions into the range of previous model estimates (Section 5); other recent assessments of both GEOS-Chem and GFED have similarly suggested that the currently implemented emission ratios fall short of observations (Andreae, 2019; Wells et al., 2014). Our observed wintertime anthropogenic NEMR falls well within the range of observations (8.4–22; Borbon et al., 2013; de Gouw et al., 2005; Goldan et al., 1995; Holzinger et al., 2001; Karl et al., 2018; Warneke et al., 2007), and suggests that the the current methanol:CO emission ratio of 0.52% in GEOS-Chem should be increased by a factor of 2, as similarly found by a recent study of field campaigns above North America (X. Chen et al., 2019). As with the pyrogenic source, this increase brings the total anthropogenic methanol emissions in GEOS-Chem into the range of previous model estimates.

In either pyrogenic or anthropogenic plumes, the NEMR may differ from the methanol:CO emission ratio due to chemical production and loss of methanol and CO in the plume during the interval between emission and sampling. Past studies have noted that the methanol NEMR in pyrogenic plumes may increase with time, likely due to secondary production (Akagi et al., 2013; Holzinger et al., 2005), although contradictory evidence exists for this source (Bruns et al., 2017). We do not observe a statistically significant dependence of methanol NEMR on plume age (Figure 5b), suggesting that secondary methanol production must occur in plumes to balance its faster oxidative loss than CO (by a factor of 4 at 298 K). This implies that our derived NEMRs reflect both emitted and secondarily produced methanol, and are not strictly emission ratios, which may explain why they tend to be higher than previous NEMRs calculated from younger plumes (Andreae & Merlet, 2001; de Gouw et al., 2006; Holzinger et al., 2005; Hornbrook et al., 2011; Lewis et al., 2013; Li et al., 2014; Simpson et al., 2011; Sinha et al., 2003, 2004; Warneke et al., 2009). However, models with low spatial resolution are unlikely to capture methanol production in plumes satisfactorily, as they necessarily dilute its precursors into large grid boxes; using an elevated emission ratio that accounts for secondary production may therefore be appropriate to quantify the overall methanol budget. Furthermore, using only fresh (<10 days) plumes for our analysis gives weighted mean pyrogenic and anthropogenic NEMRs indistinguishable within uncertainty from the weighted means unfiltered by plume age, which supports our use of the NEMR to adjust the GEOS-Chem emission ratios. While our analysis supports the possibility that secondary methanol production in pyrogenic plumes outpaces its oxidative loss relative to CO, further work (e.g., tracking of plumes over long time scales) is needed to quantify this source.

5. The Global Methanol Budget

Table 2 shows the global annual budget of tropospheric methanol from our updated simulation, after implementing the changes to methanol source terms described in Sections 3 and 4, along with comparisons to global budgets from previous studies. Figure 6 shows the contributions of methanol from individual

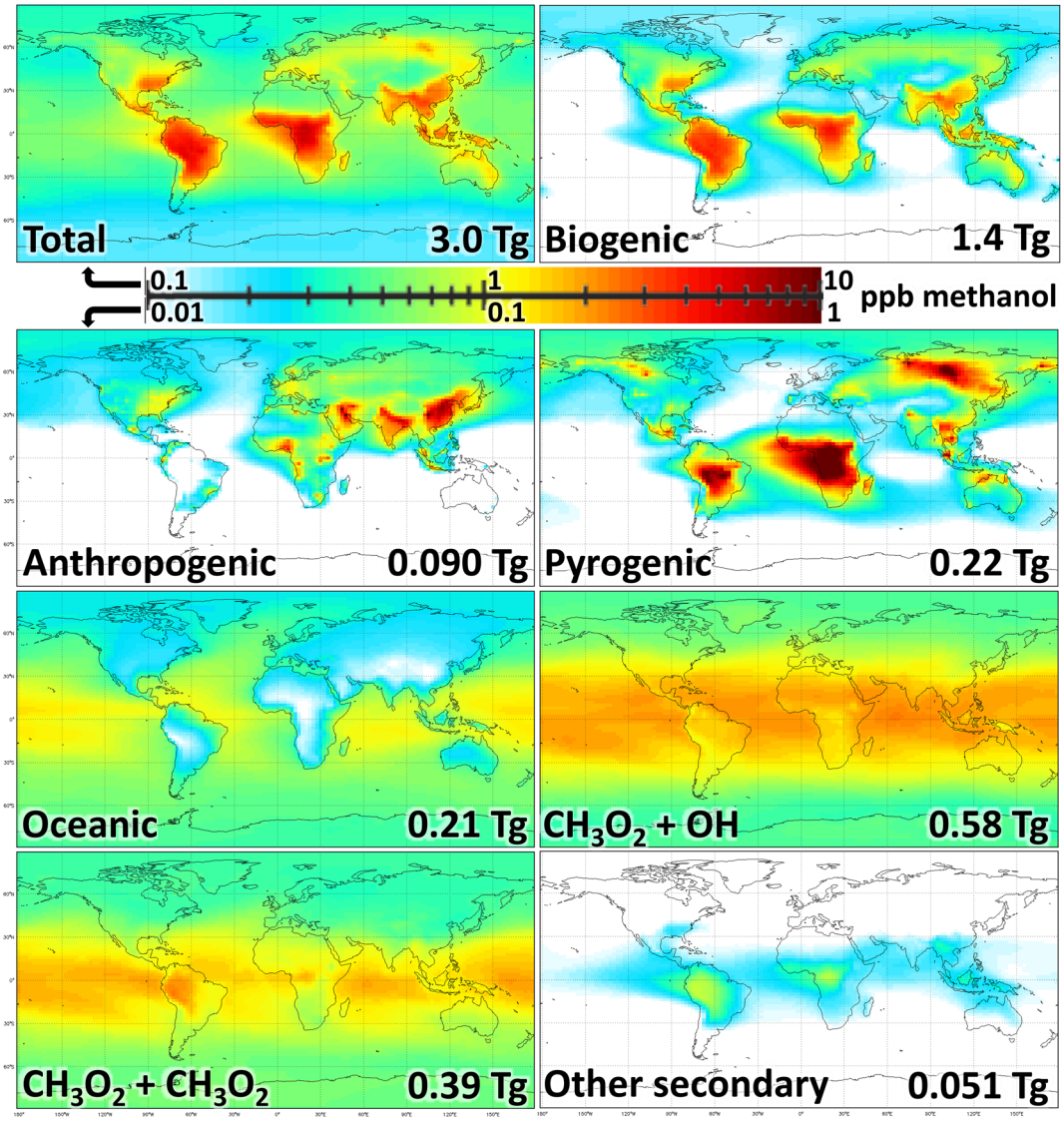

Figure 6. Methanol burden (top left) and contributions from individual sources. The maps shown annual average mixing ratios for the tropospheric column in the updated simulation. The scales for the total and biogenic panels differ from the others by a factor of 10. Numbers in the bottom right of each panel provide the annual average tropospheric burden of methanol from each source.

sources to the total tropospheric burden; corresponding zonal profiles, maps of emissions, and maps of the percent contribution from each source can be found in Figures S8–S11. We find that biogenic terrestrial emissions constitute nearly half of the tropospheric source and burden of methanol, while secondary production contributes another ~30%, with the majority of secondary production from the newly implemented CH_3O_2 + OH reaction. We calculate the total sources and sinks of methanol to be 205 Tg a^{-1}, within 5% of the median of previous estimates despite our changes to individual source terms. Our atmospheric methanol lifetime of 5.3 days and burden of 3.0 Tg are on the lower ends of the ranges of previous estimates. A more detailed listing of methanol budgets from previous studies is provided in Table S4.

The most prominent change to our methanol budget relative to previous work is the increased importance of secondary methanol production, predominantly from the inclusion of the CH_3O_2 + OH reaction, which we find provides the second largest contribution to tropospheric methanol behind biogenic emissions. Despite the corresponding decreased methanol production from the CH_3O_2 + CH_3O_2 reaction, we find a

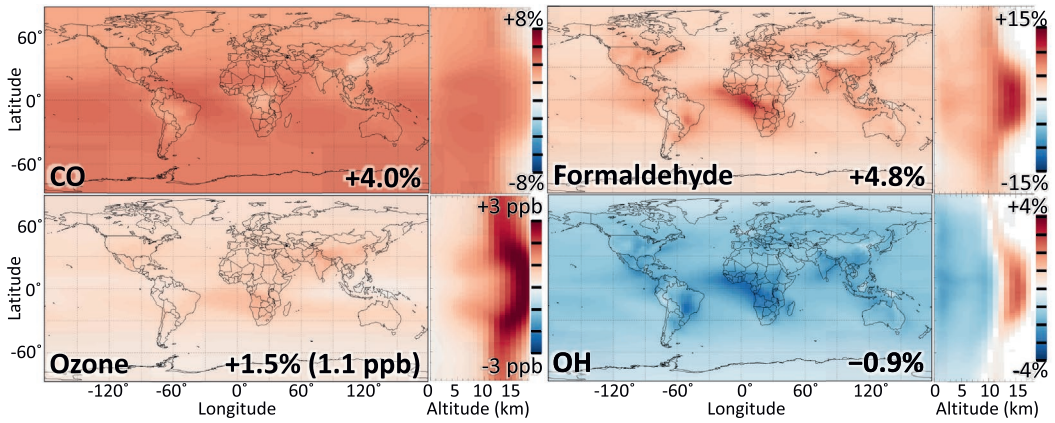

Figure 7. The role of methanol in trace gas budgets. Each panel shows changes in the annual column-average, zonal-average, and overall (numbers at bottom right) tropospheric burden of a select species due to the inclusion of methanol photochemistry in GEOS-Chem, computed by comparing the updated simulation to a sensitivity simulation in which methanol photo-oxidation is removed. The scale for ozone shows absolute changes in mixing ratio, while those for the other species are shown as percent changes.

total secondary methanol source of 60 Tg a^{-1}, 60% larger than the median from previous budgets. Müller et al. (2016), the only other study to incorporate an appreciable methanol source from the CH_3O_2 + OH reaction, found a similar total secondary methanol production of 59 Tg a^{-1}. Jacob et al. (2005) proposed that a secondary methanol source of 50–100 Tg a^{-1}, higher than mechanisms known at the time could provide, would alleviate negative model biases over the tropical Western Pacific. Thus, our increased secondary contribution to the methanol budget remains consistent with previous work.

The other notable change to the methanol budget introduced here is the reduced gross oceanic source due to our lower seawater methanol concentration and updated parameterization of transfer velocities. While we simulate a similar small net flux of methanol to the ocean (14 Tg a^{-1}) to previous studies (median 10 Tg a^{-1}), our gross oceanic emission of 24 Tg a^{-1} is only 60% as large as the median of previous estimates and 30% as large as in Millet et al. (2008). This also causes a reduction in the gross uptake of methanol by the ocean, because most ocean-derived methanol is rapidly lost again to the sea surface. Because of this rapid oceanic uptake, equivalent to a mean deposition velocity of 0.67 cm s^{-1} across the ocean surface, the ocean-derived methanol has a short lifetime, as previously shown in situ by Yang, Blomquist et al. (2014). Ocean-derived methanol is therefore a minor contributor to the methanol budget even in the marine boundary layer, where the secondary source (including subsiding from above) dominates (see Figure 2). Indeed, we find that the atmospheric lifetime of ocean-derived methanol (3.2 days) is much smaller than that of methanol from other sources (5.5 days); as a result, although gross ocean emission provides 12% of the total atmospheric methanol source in our updated simulation, it only contributes 7% of the tropospheric methanol burden.

5.1. Implications of Methanol Chemistry

Due to its ubiquity as the troposphere's most abundant nonmethane VOC, methanol can have important implications for the budgets of additional trace gases of interest. Figure 7 shows the changes in tropospheric OH, ozone, formaldehyde, and CO due to methanol photochemistry, computed as the difference between simulations without and with the methanol + OH and methanol + Cl reactions (using the updated methanol sources). Methanol oxidation contributes 4.0% of the tropospheric CO burden and 4.8% of the formaldehyde burden, and increases the surface ozone burden by 1.0%. It also causes a 0.9% reduction in tropospheric OH, thus augmenting the lifetime of other trace gases such as methane.

These impacts are not uniformly distributed throughout the atmosphere. For example, the OH reduction due to methanol photooxidation is strongest in the boundary layer (1.8%), and reaches up to 4% in areas with high biogenic methanol emissions. Conversely, due to its long lifetime against oxidation, methanol

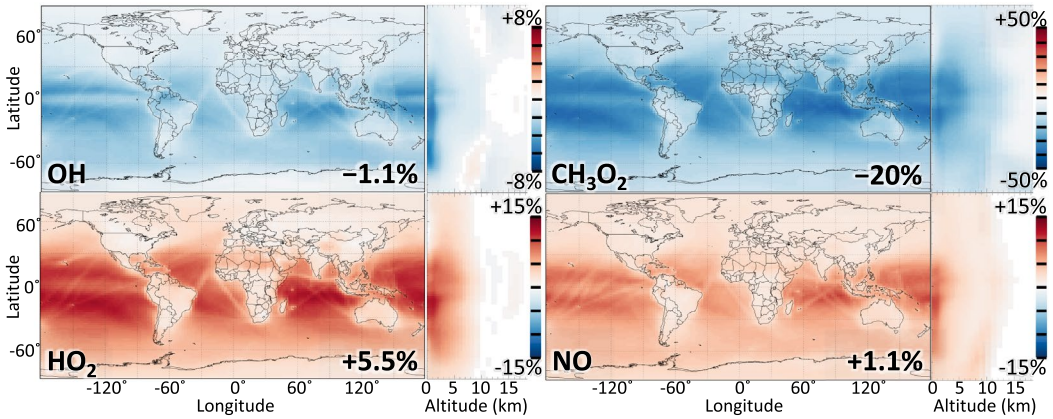

Figure 8. The role of the CH_3O_2 + OH reaction in radical budgets. Each panel shows changes in the annual column-average, zonal-average, and overall (number at bottom right) tropospheric burden of a select species due to the inclusion of the CH_3O_2 + OH reaction in GEOS-Chem, computed by comparing the updated simulation to a sensitivity simulation in which the reaction in question is removed.

plays its most prominent role in trace gas budgets in the tropical upper troposphere. There, methanol contributes up to 14% of the formaldehyde burden; subsequent radical production from the photolysis of this formaldehyde increases OH by 5%. More details on the spatial patterns of these changes are given in Table S5, while Figure S12 shows the changes due solely to primary methanol emissions, which are similar in pattern to those in Figure 7 but smaller in magnitude.

Finally, the implementation of the CH_3O_2 + OH reaction in the GEOS-Chem chemical mechanism alters tropospheric radical budgets, particularly over the tropical oceans where the CH_3O_2 lifetime is longest. The spatial patterns of these changes are shown in Figure 8. Globally, the CH_3O_2 + OH reaction represents 14% of the fate of CH_3O_2 radicals, behind only reaction with NO (44%) and HO_2 (38%) in our updated simulation. The direct consequences of this reaction are decreases in the annual average tropospheric burdens of CH_3O_2 and OH by 20% and 1.1%, respectively, reaching local maxima of 45% and 7% in the tropical ocean boundary layer. These decreases have secondary effects on the budgets of their other reaction partners, most notably HO_2 and NO, whose tropospheric burdens increase by 5.5% and 1.1%, respectively (up to 14% and 11% locally). Additional impacts of the CH_3O_2 + OH reaction, including changes to formaldehyde, CO, ozone, and methyl hydroperoxide, are provided in Table S5 and Figure S13.

The CH_3O_2 + OH reaction also contributes to OH reactivity, which Thames et al. (2020) and Travis et al. (2020) showed was underestimated relative to ATom measurements in simulations using the Master Chemical Mechanism v3.3.1 and GEOS-Chem v12.3.0, respectively. Neither mechanism included the CH_3O_2 + OH reaction, which contributes most to OH reactivity in the marine boundary layer, precisely where the missing OH reactivity is highest. Our simulations suggest that the CH_3O_2 + OH reaction directly contributes/*sim*0.1 s^{-1} of additional OH reactivity in the marine boundary layer, and is therefore insufficient to make up the 0.4–0.7 s^{-1} mean missing reactivity (Thames et al., 2020). However, the contribution of this novel reaction pathway could be increased by including other RO_2 + OH reactions, and by considering secondary effects of CH_3O_2 + OH on OH reactivity via perturbations in the concentrations of other OH reaction partners (e.g., increased methanol, CO, and HO_2). Further analysis is required to determine the balance of these effects and their influences on OH reactivity.

6. Conclusions

We have used observations from the ATom aircraft campaign over the Pacific and Atlantic Oceans, simulated with source-tagged tracers in the GEOS-Chem model, to better understand the factors controlling methanol concentrations in the remote oceanic atmosphere. From there we constructed a new global budget for methanol and examined the implications for global atmospheric chemistry.

We find that background methanol concentrations in the remote oceanic atmosphere (200–400 pptv) are mostly controlled by chemical production from the CH_3O_2 + OH and CH_3O_2 + CH_3O_2 reactions (global sources of 33 and 24 Tg a^{-1}, respectively). The CH_3O_2 + OH reaction is generally not included in global models of atmospheric chemistry, but our results indicate that it produces methanol with 13% yield and more broadly impacts hydrogen oxide (HO_x) radical budgets. Air-sea exchange is optimized with a surface ocean methanol concentration of 61 nM, resulting in the ocean representing a weak net sink (14 Tg a^{-1}). Although our derived sea-surface methanol concentration and gross unidirectional fluxes of methanol between the ocean and atmosphere are sensitive to uncertain coefficients within the model's air-sea exchange parameterization, we find that the net flux is well constrained by our fitting. Contrary to previous atmospheric modeling results, but consistent with recent flux measurements over the Atlantic Ocean (Yang, Blomquist et al., 2014; Yang et al., 2013), we show that the gross ocean emission of methanol (here 24 Tg a^{-1}) does not control methanol concentrations in the marine atmosphere, even in the boundary layer, because of rapid deposition and the role of chemical production.

The ATom observations also included a number of anthropogenic and biomass burning plumes containing elevated methanol. From correlations with CO, we inferred global anthropogenic and biomass burning emissions of 6.3 and 13 Tg a^{-1}, respectively, at the high end of current estimates. The methanol relative enhancement in biomass burning plumes did not significantly change over prolonged aging, suggesting that chemical production in the plumes compensates for loss from oxidation.

The resulting global budget of methanol constructed from our analysis has a global source of 205 Tg a^{-1} including 101 Tg a^{-1} from the terrestrial biosphere and 60 Tg a^{-1} from chemical production. Ocean, biomass burning, and anthropogenic activities are additional minor sources. The global atmospheric lifetime of methanol is 5.3 days, with oxidation and deposition each contributing about half of the sink. The secondary source from chemical production accounts for 29% of the global source of methanol but 34% of the global burden because it is less sensitive to deposition than the others. Sensitivity simulations with GEOS-Chem show that accounting for methanol chemistry increases global tropospheric CO, formaldehyde, and ozone by 4.0%, 4.8%, and 1.5%, respectively, and decreases global tropospheric OH by 0.9%. Methanol chemistry aside, including the CH_3O_2 + OH reaction in GEOS-Chem has significant impact on global budgets including for OH (−1.1%), CH_3O_2 (−20%), HO_2 (+5.5%), and NO (+1.1%).

Data Availability Statement

Data from the NASA Atmospheric Tomography mission are available at https://doi.org/10.3334/ORNLDAAC/1581.

Acknowledgments
This work was supported by the US NSF Atmospheric Chemistry Program, by the NASA Atmospheric Composition Modeling and Analysis Program, and by the US EPA Science to Achieve Results Program. We thank Bruce Daube and Kathryn McKain for their contribution to the collection of CO data on ATom. K. H. B. acknowledges additional support from the Harvard University Center for the Environment and the National Oceanic and Atmospheric Administration's Climate and Global Change Fellowship programs. D. B. M., X. C., and K. C. W. acknowledge support from the NASA Atmospheric Composition Campaign Data Analysis and Modeling (ACCDAM) program (Grant no. NNX14AP89G). This material is based upon work supported by the National Center for Atmospheric Research, which is a major facility sponsored by the National Science Foundation under Cooperative Agreement No. 1852977. All ATom data used in this study can be accessed via https://daac.ornl.gov/ATOM/campaign/.

References

Akagi, S. K., Yokelson, R. J., Burling, I. R., Meinardi, S., Simpson, I., Blake, D. R., et al. (2013). Measurements of reactive trace gases and variable O_3 formation rates in some South Carolina biomass burning plumes. *Atmospheric Chemistry and Physics*, *13*, 1141–1165. https://doi.org/10.5194/acp-13-1141-2013

Akagi, S. K., Yokelson, R. J., Wiedinmyer, C., Alvarado, M. J., Reid, J. S., Karl, T., et al. (2011). Emission factors for open and domestic biomass burning for use in atmospheric models. *Atmospheric Chemistry and Physics*, *11*, 4039–4072. https://doi.org/10.5194/acp-11-4039-2011

Andreae, M. O. (2019). Emission of trace gases and aerosols from biomass burning—An updated assessment. *Atmospheric Chemistry and Physics*, *19*, 8523–8546. https://doi.org/10.5194/acp-19-8523-2019

Andreae, M. O., & Merlet, P. (2001). Emission of trace gases and aerosols from biomass burning. *Global Biogeochemical Cycles*, *15*, 955–966. https://doi.org/10.1029/2000GB001382

Apel, E. C., Emmons, L. K., Karl, T., Flocke, F., Hills, A. J., Madronich, S., et al. (2010). Chemical evolution of volatile organic compounds in the outflow of the Mexico City Metropolitan area. *Atmospheric Chemistry and Physics*, *10*, 2353–2375. https://doi.org/10.5194/acp-10-2353-2010

Apel, E. C., Hills, A. J., Lueb, R., Zindel, S., Eisele, S., & Riemer, D. D. (2003). A fast-GC/MS system to measure C_2 to C_4 carbonyls and methanol aboard aircraft. *Journal of Geophysical Research*, *108*,D208794. https://doi.org/10.1029/2002JD003199

Apel, E. C., Hornbrook, R. S., Hills, A. J., Blake, N. J., Barth, M. C., Weinheimer, A., et al. (2015). Upper tropospheric ozone production from lightning NO_x-impacted convection: Smoke ingestion case study from the DC3 campaign. *Journal of Geophysical Research: Atmospheres*, *120*, 2505–2523. https://doi.org/10.1002/2014JD022121

Archibald, A. T., Petit, A. S., Percival, C. J., Harvey, J. N., & Shallcross, D. E. (2009). On the importance of the reaction between OH and RO_2 radicals. *Atmospheric Science Letters*, *10*, 102–108. https://doi.org/10.1002/asl.216

Arrieta, J. M., Duarte, C. M., Sala, M. M., & Dachs, J. (2016). Out of thin air: Microbial utilization of atmospheric gaseous organics in the surface ocean. *Frontiers in Microbiology*, *6*, 1566. https://doi.org/10.3389/fmicb.2015.01566

Ashworth, K., Chung, S. H., McKinney, K. A., Liu, Y., Munger, J. W., Martin, S. T., & Steiner, A. L. (2016). Modelling bidirectional fluxes of methanol and acetaldehyde with the FORCAsT canopy exchange model. *Atmospheric Chemistry and Physics*, *16*, 15461–15484. https://doi.org/10.5194/acp-16-15461-2016

Assaf, E., Sheps, L., Whalley, L., Heard, D., Tomas, A., Schoemaecker, C., & Fittschen, C. (2017). The reaction between CH_3O_2 and OH radicals: Product yields and atmospheric implications. *Environmental Science & Technology*, *51*, 2170–2177. https://doi.org/10.1021/acs.est.6b06265

Assaf, E., Song, B., Tomas, A., Schoemaecker, C., & Fittschen, C. (2016). Rate constant of the reaction between CH_3O_2 radicals and OH radicals revisited. *Journal of Physical Chemistry A*, *120*, 8923–8932. https://doi.org/10.1021/acs.jpca.6b07704

Atkinson, R., Baulch, D. L., Cox, R. A., Crowley, J. N., Hampson, R. F., Hynes, R. G., ... Subcommittee, I. (2006). Evaluated kinetic and photochemical data for atmospheric chemistry: Volume II - gas phase reactions of organic species. *Atmospheric Chemistry and Physics*, *6*, 3625–4055. https://doi.org/10.5194/acp-6-3625-2006

Bader, W., Stavrakou, T., Muller, J.-F., Reimann, S., Boone, C. D., Harrison, J. J., et al. (2014). Long-term evolution and seasonal modulation of methanol above Jungfraujoch (46.5°N, 8.0°E): Optimisation of the retrieval strategy, comparison with model simulations and independent observations. *Atmospheric Measurement Techniques*, *7*, 3861–3872. https://doi.org/10.5194/amt-7-3861-2014

Bates, K. H., & Jacob, D. J. (2019). A new model mechanism for atmospheric oxidation of isoprene: Global effects on oxidants, nitrogen oxides, organic products, and secondary organic aerosol. *Atmospheric Chemistry and Physics*, *19*, 9613–9640. https://doi.org/10.5194/acp-19-9613-2019

Beale, R., Dixon, J. L., Arnold, S. R., Liss, P. S., & Nightingale, P. D. (2013). Methanol, acetaldehyde, and acetone in the surface waters of the Atlantic Ocean. *Journal of Geophysical Research: Oceans*, *118*, 5412–5425. https://doi.org/10.1002/jgrc.20322

Beale, R., Dixon, J. L., Smyth, T. J., & Nightingale, P. D. (2015). Annual study of oxygenated volatile organic compounds in UK shelf waters. *Marine Chemistry*, *171*, 96–106. https://doi.org/10.1016/j.marchem.2015.02.013

Beale, R., Liss, P. S., Dixon, J. L., & Nightingale, P. D. (2011). Quantification of oxygenated volatile organic compounds in seawater by membrane inlet-proton transfer reaction/mass spectrometry. *Analytica Chimica Acta*, *706*, 128–134. https://doi.org/10.1016/j.aca.2011.08.023

Borbon, A., Gilman, J. B., Kuster, W. C., Grand, N., Chevaillier, S., Colomb, A., et al. (2013). Emission ratios of anthropogenic volatile organic compounds in northern mid-latitude megacities: Observations versus emission inventories in Los Angeles and Paris. *Journal of Geophysical Research: Atmospheres*, *118*, 2041–2057. https://doi.org/10.1002/jgrd.50059

Bossolasco, A., Faragó, E. P., Schoemaecker, C., & Fittscher, C. (2014). Rate constant of the reaction between CH_3O_2 and OH radicals. *Chemical Physics Letters*, *593*, 7–13. https://doi.org/10.1016/j.cplett.2013.12.052

Brewer, J. F., Fischer, E. V., Commane, R., Wofsy, S. C., Daube, B., Apel, E. C., et al. (2020). Evidence for an oceanic source of methyl ethyl ketone to the atmosphere. *Geophysical Research Letters*, *47*, e2019GL086045. https://doi.org/10.1029/2019GL086045

Bruns, E. A., Slowik, J. G., El Haddad, I., Kilic, D., Klein, F., Dommen, J., et al. (2017). Characterization of gas-phase organics using proton transfer reaction time-of-flight mass spectrometry: Fresh and aged residential wood combustion emissions. *Atmospheric Chemistry and Physics*, *17*, 705–720. https://doi.org/10.5194/acp-17-705-2017

Butkovskaya, N., Rayez, M.-T., Rayez, J.-C., Kukui, A., & Le Bras, G. (2009). Water vapor effect on the HNO_3 yields in the HO_2 + NO reaction: experimental and theoretical evidence. *Journal of Physical Chemistry A*, *113*, 11327–11342. https://doi.org/10.1021/jp811428p

Caravan, R. L., Khan, M. A. H., Zádor, J., Sheps, L., Antonov, I. O., Rotavera, B., et al. (2018). The reaction of hydroxyl and methylperoxy radicals is not a major source of atmospheric methanol. *Nature Communications*, *9*, 4343. https://doi.org/10.1038/s41467-018-06716-x

Carpenter, L. J., Lewis, A. C., Hopkins, J. R., Read, K. A., Longley, I. D., & Gallagher, M. W. (2004). Uptake of methanol to the North Atlantic Ocean surface. *Global Biogeochemical Cycles*, *18*, GB4027. https://doi.org/10.1029/2004GB002294

Chao, W., Lin, J. J.-M., Takahashi, K., Tomas, A., Yu, L., Kajii, Y., et al. (2019). Water vapor does not catalyze the reaction between methanol and OH radicals. *Angewandte Chemie International Edition*, *58*(15), 5013–5017. https://doi.org/10.1002/anie.201900711

Chen, X., Millet, D. B., Singh, H. B., Wisthaler, A., Apel, E. C., Atlas, E. L., et al. (2019). On the sources and sinks of atmospheric VOCs: An integrated analysis of recent aircraft campaigns over North America. *Atmospheric Chemistry and Physics*, *19*, 9097–9123. https://doi.org/10.5194/acp-19-9097-2019

Chen, Q., Schmidt, J. A., Shah, V., Jaeglé, L., Sherwen, T., & Alexander, B. (2017). Sulfate production by reactive bromine: Implications for the global sulfur and reactive bromine budgets. *Geophysical Research Letters*, *44*, 7069–7078. https://doi.org/10.1002/2017GL073812

de Gouw, J. A., Middlebrook, A. M., Warneke, C., Goldan, P. D., Kuster, W. C., Roberts, J. M., et al. (2005). Budget of organic carbon in a polluted atmosphere: Results from the New England Air Quality Study in 2002. *Journal of Geophysical Research*, *110*, D16305. https://doi.org/10.1029/2004JD005623

de Gouw, J. A., Warneke, C., Stohl, A., Wollny, A. G., Brock, C. A., Cooper, O. R., et al. (2006). Volatile organic compounds composition of merged and aged forest fire plumes from Alaska and Western Canada. *Journal of Geophysical Research*, *111*(D10), 303. https://doi.org/10.1029/2005JD006175

Deng, W., Peng, L., Jiao, N., & Zhang, Y. (2018). Differential incorporation of one-carbon substrates among microbial populations identified by stable isotope probing from the estuary to South China Sea. *Scientific Reports*, *8*, 15378. https://doi.org/10.1038/s41598-018-33497-6

Dinasquet, J., Tiirola, M., & Azam, F. (2018). Enrichment of bacterioplankton able to utilize one-carbon and methylated compounds in the coastal Pacific Ocean. *Frontiers in Marine Science*, *5*, 307. https://doi.org/10.3389/fmars.2018.00307

Diskin, G. S., Podolske, J. R., Sachse, G. W., & Slate, T. A. (2002). Open-path airborne tunable diode laser hygrometer. In A. Fried (Ed.), Diode lasers and applications in atmospheric sensing (Vol. 4817, pp. 196–204). SPIE. https://doi.org/10.1117/12.453736

Dixon, J. L., Beale, R., & Nightingale, P. D. (2011a). Microbial methanol uptake in northeast Atlantic waters. *The ISME Journal*, *5*, 704–716. https://doi.org/10.1038/ismej.2010.169

Dixon, J. L., Beale, R., & Nightingale, P. D. (2011b). Rapid biological oxidation of methanol in the tropical Atlantic: significance as a microbial carbon source. *Biogeosciences*, *8*, 2707–2716. https://doi.org/10.5194/bg-8-2707-2011

Dixon, J. L., & Nightingale, P. D. (2012). Fine-scale variability in methanol uptake and oxidation: from the microlayer to 1000 m. *Biogeosciences*, *9*, 2961–2972. https://doi.org/10.5194/bg-9-2961-2012

Dixon, J. L., Sargeant, S., Nightingale, P. D., & Colin Murrell, J. (2013). Gradients in microbial methanol uptake: Productive coastal upwelling waters to oligotrophic gyres in the Atlantic Ocean. *The ISME Journal*, *7*, 568–580. https://doi.org/10.1038/ismej.2012.130

Dufour, G., Boone, C. D., Rinsland, C. P., & Bernath, P. F. (2006). First space-borne measurements of methanol inside aged southern tropical to mid-latitude biomass burning plumes using the ACE-FTS instrument. *Atmospheric Chemistry and Physics*, *6*, 3463–3470. https://doi.org/10.5194/acp-6-3463-2006

Duncan, B. N., Logan, J. A., Bey, I., Megretskaia, I. A., Yantosca, R. M., Novelli, P. C., et al. (2007). Global budget of CO, 1988–1997: Source estimates and validation with a global model. *Journal of Geophysical Research*, *112*, D22301. https://doi.org/10.1029/2007JD008459

Eastham, S. D., & Jacob, D. J. (2017). Limits on the ability of global Eulerian models to resolve intercontinental transport of chemical plumes. *Atmospheric Chemistry and Physics*, *17*, 2543–2553. https://doi.org/10.5194/acp-17-2543-2017

Eastham, S. D., Weisenstein, D. K., & Barrett, S. R. (2014). Development and evaluation of the unified tropospheric-stratospheric chemistry extension (UCX) for the global chemistry-transport model GEOS-Chem. *Atmospheric Environment*, *89*, 52–63. https://doi.org/10.1016/j.atmosenv.2014.02.001

Fall, R., & Benson, A. A. (1996). Leaf methanol—The simplest natural product from plants. *Trends in Plant Science*, *1*, 296–301. https://doi.org/10.1016/S1360-1385(96)88175-0

Ferracci, V., Heimann, I., Abraham, N. L., Pyle, J. A., & Archibald, A. T. (2018). Global modelling of the total OH reactivity: investigations on the "missing" OH sink and its atmospheric implications. *Atmospheric Chemistry and Physics*, *18*, 7109–7129. https://doi.org/10.5194/acp-18-7109-2018

Fischer, E. V., Jacob, D. J., Millet, D. B., Yantosca, R. M., & Mao, J. (2012). The role of the ocean in the global atmospheric budget of acetone. *Geophysical Research Letters*, *39*, L01807. https://doi.org/10.1029/2011GL050086

Fisher, J. A., Atlas, E. L., Barletta, B., Meinardi, S., Blake, D. R., Thompson, C. R., et al. (2018). Methyl, ethyl, and propyl nitrates: global distribution and impacts on reactive nitrogen in remote marine environments. *Journal of Geophysical Research: Atmospheres*, *123*, 12429–12451. https://doi.org/10.1029/2018JD029046

Fittschen, C., Whalley, L. K., & Heard, D. E. (2014). The reaction of CH_3O_2 radicals with OH radicals: A neglected sink for CH_3O_2 in the remote atmosphere. *Environmental Science & Technology*, *48*, 7700–7701. https://doi.org/10.1021/es502481q

Fukui, Y., & Doskey, P. V. (1998). Air-surface exchange of nonmethane organic compounds at a grassland site: Seasonal variations and stressed emissions. *Journal of Geophysical Research*, *103*, 13153–13168. https://doi.org/10.1029/98JD00924

Galbally, I. E., & Kirstine, W. (2002). The production of methanol by flowering plants and the global cycle of methanol. *Journal of Atmospheric Chemistry*, *43*, 195–229. https://doi.org/10.1023/A:1020684815474

Giglio, L., Randerson, J. T., & van der Werf, G. R. (2013). Analysis of daily, monthly, and annual burned area using the fourth-generation global fire emissions database (GFED4). *Journal of Geophysical Research: Biogeosciences*, *118*, 317–328. https://doi.org/10.1002/jgrg.20042@

Giovannoni, S. J., Hayakawa, D. H., Tripp, H. J., Stingl, U., Givan, S. A., Cho, J.-C., et al. (2008). The small genome of an abundant coastal ocean methylotroph. *Environmental Microbiology*, *10*, 1771–1782. https://doi.org/10.1111/j.1462-2920.2008.01598.x

Goldan, P. D., Trainer, M., Kuster, W. C., Parrish, D. D., Carpenter, J., Roberts, J. M., et al. (1995). Measurements of hydrocarbons, oxygenated hydrocarbons, carbon monoxide, and nitrogen oxides in an urban basin in Colorado: Implications for emission inventories. *Journal of Geophysical Research*, *100*, 22771–22783. https://doi.org/10.1029/95JD01369

Guenther, A., Jiang, X., Heald, C. L., Sakulyanontvittaya, T., Duhl, T., Emmons, L. K., & Wang, X. (2012). The Model of Emissions of Gases and Aerosols from Nature version 2.1 (MEGAN 2.1): An extended and updated framework for modeling biogenic emissions. *Geoscientific Model Development*, *5*(6), 1471–1492.

Guenther, A., Karl, T., Harley, P., Wiedinmyer, C., Palmer, P. I., & Geron, C. (2006). Estimates of global terrestrial isoprene emissions using MEGAN (Model of Emissions of Gases and Aerosols from Nature). *Atmospheric Chemistry and Physics*, *6*, 3181–3210. https://doi.org/10.5194/acp-6-3181-2006

Harley, P., Greenberg, J., Niinemets, U., & Guenther, A. (2007). Environmental controls over methanol emission from leaves. *Biogeosciences*, *4*, 1083–1099. https://doi.org/10.5194/bg-4-1083-2007

Heikes, B. G., Chang, W., Pilson, M. E. Q., Swift, E., Singh, H. B., Guenther, A., et al. (2002). Atmospheric methanol budget and ocean implication. *Global Biogeochemical Cycles*, *16*, 1–13. https://doi.org/10.1029/2002GB001895

Holzinger, R., Jordan, A., Hansel, A., & Lindinger, W. (2001). Methanol measurements in the lower troposphere near Innsbruck (47.16°N; 11.24°E), Austria. *Atmospheric Environment*, *35*, 2525–2532. https://doi.org/10.1016/S1352-2310(00)00430-1

Holzinger, R., Williams, J., Salisbury, G., Klüpfel, T., de Reus, M., Traub, M., et al. (2005). Oxygenated compounds in aged biomass burning plumes over the Eastern Mediterranean: Evidence for strong secondary production of methanol and acetone. *Atmospheric Chemistry and Physics*, *5*, 39–46. https://doi.org/10.5194/acp-5-39-2005

Hornbrook, R. S., Blake, D. R., Diskin, G. S., Fried, A., Fuelberg, H. E., Meinardi, S., et al. (2011). Observations of nonmethane organic compounds during ARCTAS—Part 1: Biomass burning emissions and plume enhancements. *Atmospheric Chemistry and Physics*, *11*, 11103–11130. https://doi.org/10.5194/acp-11-11103-2011

Jacob, D. J., Field, B. D., Li, Q., Blake, D. R., de Gouw, J., Warneke, C., et al. (2005). Global budget of methanol: constraints from atmospheric observations. *Journal of Geophysical Research*, *110*, D08303. https://doi.org/10.1029/2004JD005172

Jara-Toro, R. A., Hernández, F. J., Taccone, R. A., Lane, S. I., & Pino, G. A. (2017). Water catalysis of the reaction between methanol and OH at 294 K and the atmospheric implications. *Angewandte Chemie International Edition*, *56*, 2166–2170. https://doi.org/10.1002/anie.201612151

Johnson, M. T. (2010). A numerical scheme to calculate temperature and salinity dependent air-water transfer velocities for any gas. *Ocean Science*, *6*, 913–920. https://doi.org/10.5194/os-6-913-2010

Kameyama, S., Tanimoto, H., Inomata, S., Tsunogai, U., Ooki, A., Takeda, S., et al. (2010). High-resolution measurement of multiple volatile organic compounds dissolved in seawater using equilibrator inlet–proton transfer reaction-mass spectrometry (EI–PTR-MS). *Marine Chemistry*, *122*, 59–73. https://doi.org/10.1016/j.marchem.2010.08.003

Karl, T., Guenther, A., Spirig, C., Hansel, A., & Fall, R. (2003). Seasonal variation of biogenic VOC emissions above a mixed hardwood forest in northern Michigan. *Geophysical Research Letters*, *30*, 2186. https://doi.org/10.1029/2003GL018432

Karl, T., Harley, P., Emmons, L., Thornton, B., Guenther, A., Basu, C., et al. (2010). Efficient atmospheric cleansing of oxidized organic trace gases by vegetation. *Science*, *330*(6005), 816–819. https://doi.org/10.1126/science.1192534

Karl, T., Harley, P., Guenther, A., Rasmussen, R., Baker, B., Jardine, K., & Nemitz, E. (2005). The bi-directional exchange of oxygenated VOCs between a loblolly pine (pinus taeda) plantation and the atmosphere. *Atmospheric Chemistry and Physics*, *5*, 3015–3031. https://doi.org/10.5194/acp-5-3015-2005

Karl, T., Potosnak, M., Guenther, A., Clark, D., Walker, J., Herrick, J. D., & Geron, C. (2004). Exchange processes of volatile organic compounds above a tropical rain forest: Implications for modeling tropospheric chemistry above dense vegetation. *Journal of Geophysical Research*, *109*, D18306. https://doi.org/10.1029/2004JD004738

Karl, T., Striednig, M., Graus, M., Hammerle, A., & Wohlfahrt, G. (2018). Urban flux measurements reveal a large pool of oxygenated volatile organic compound emissions. *Proceedings of the National Academy of Sciences of the United States of America*, *115*(6), 1186–1191. https://doi.org/10.1073/pnas.1714715115

Khan, M., Cooke, M., Utembe, S., Archibald, A., Derwent, R., Jenkin, M., et al. (2015). Global analysis of peroxy radicals and peroxy radical-water complexation using the STOCHEM-CRI global chemistry and transport model. *Atmospheric Environment*, *106*, 278–287. https://doi.org/10.1016/j.atmosenv.2015.02.020

Khan, M., Cooke, M., Utembe, S., Xiao, P., Derwent, R., Jenkin, M., et al. (2014). Reassessing the photochemical production of methanol from peroxy radical self and cross reactions using the STOCHEM-CRI global chemistry and transport model. *Atmospheric Environment*, *99*, 77–84. https://doi.org/10.1016/j.atmosenv.2014.09.056

Kirstine, W., Galbally, I., Ye, Y., & Hooper, M. (1998). Emissions of volatile organic compounds (primarily oxygenated species) from pasture. *Journal of Geophysical Research*, *103*, 10605–10619. https://doi.org/10.1029/97JD03753

Lamarque, J.-F., Bond, T. C., Eyring, V., Granier, C., Heil, A., Klimont, Z., et al. (2010). Historical (1850-2000) gridded anthropogenic and biomass burning emissions of reactive gases and aerosols: Methodology and application. *Atmospheric Chemistry and Physics*, *10*, 7017–7039. https://doi.org/10.5194/acp-10-7017-2010

Legreid, G., Lööv, J. B., Staehelin, J., Hueglin, C., Hill, M., Buchmann, B., et al. (2007). Oxygenated volatile organic compounds (OVOCs) at an urban background site in Zürich (Europe): Seasonal variation and source allocation. *Atmospheric Environment*, *41*, 8409–8423. https://doi.org/10.1016/j.atmosenv.2007.07.026

Lewis, A. C., Evans, M. J., Hopkins, J. R., Punjabi, S., Read, K. A., Purvis, R. M., et al. (2013). The influence of biomass burning on the global distribution of selected non-methane organic compounds. *Atmospheric Chemistry and Physics*, *13*, 851–867. https://doi.org/10.5194/acp-13-851-2013

Li, L., Chen, Y., Zeng, L., Shao, M., Xie, S., Chen, W., et al. (2014). Biomass burning contribution to ambient volatile organic compounds (VOCs) in the Chengdu-Chongqing Region (CCR), China. *Atmospheric Environment*, *99*, 403–410. https://doi.org/10.1016/j.atmosenv.2014.09.067

Liss, P., & Slater, P. (1974). Flux of gases across the air-sea interface. *Nature*, *247*, 181–184. https://doi.org/10.1038/247181a0

MacDonald, R. C., & Fall, R. (1993). Detection of substantial emissions of methanol from plants to the atmosphere. *Atmospheric Environment*, *27*, 1709–1713. https://doi.org/10.1016/0960-1686(93)90233-O

Madronich, S., & Calvert, J. G. (1990). Permutation reactions of organic peroxy radicals in the troposphere. *Journal of Geophysical Research*, *95*, 5697–5715. https://doi.org/10.1029/JD095iD05p05697

Magneron, I., Mellouki, A., Le Bras, G., Moortgat, G. K., Horowitz, A., & Wirtz, K. (2005). Photolysis and OH-initiated oxidation of glycolaldehyde under atmospheric conditions. *Journal of Physical Chemistry A*, *109*, 4552–4561. https://doi.org/10.1021/jp044346y

Mao, H., Talbot, R., Nielsen, C., & Sive, B. (2006). Controls on methanol and acetone in marine and continental atmospheres. *Geophysical Research Letters*, *33*, L02803. https://doi.org/10.1029/2005GL024810

Mauzerall, D. L., Logan, J. A., Jacob, D. J., Anderson, B. E., Blake, D. R., Bradshaw, J. D., et al. (1998). Photochemistry in biomass burning plumes and implications for tropospheric ozone over the tropical South Atlantic. *Journal of Geophysical Research*, *103*(D7), 8401–8423. https://doi.org/10.1029/97JD02612

McManus, J. B., Nelson, D. D., Shorter, J. H., Jimenez, R., Herndon, S., Saleska, S., & Zahniser, M. (2005). A high precision pulsed quantum cascade laser spectrometer for measurements of stable isotopes of carbon dioxide. *Journal of Modern Optics*, *52*, 2309–2321. https://doi.org/10.1080/09500340500303710

Millet, D. B., Baasandorj, M., Farmer, D. K., Thornton, J. A., Baumann, K., Brophy, P., et al. (2015). A large and ubiquitous source of atmospheric formic acid. *Atmospheric Chemistry and Physics*, *15*, 6283–6304. https://doi.org/10.5194/acp-15-6283-2015

Millet, D. B., Jacob, D. J., Custer, T. G., de Gouw, J. A., Goldstein, A. H., Karl, T., et al. (2008). New constraints on terrestrial and oceanic sources of atmospheric methanol. *Atmospheric Chemistry and Physics*, *8*, 6887–6905. https://doi.org/10.5194/acp-8-6887-2008

Mincer, T. J., & Aicher, A. C. (2016). Methanol production by a broad phylogenetic array of marine phytoplankton. *PloS One*, *11*, 1–17. https://doi.org/10.1371/journal.pone.0150820

Mu, M., Randerson, J. T., van der Werf, G. R., Giglio, L., Kasibhatla, P., Morton, D., et al. (2011). Daily and 3-hourly variability in global fire emissions and consequences for atmospheric model predictions of carbon monoxide. *Journal of Geophysical Research*, *116*, D24303. https://doi.org/10.1029/2011JD016245

Müller, J.-F., Liu, Z., Nguyen, V. S., Stavrakou, T., Harvey, J. N., & Peeters, J. (2016). The reaction of methyl peroxy and hydroxyl radicals as a major source of atmospheric methanol. *Nature Communications*, *7*, 13213. https://doi.org/10.1038/ncomms13213

Nemecek-Marshall, M., MacDonald, R. C., Franzen, J. J., Wojciechowski, C. L., & Fall, R. (1995). Methanol emission from leaves (enzymatic detection of gas-phase methanol and relation of methanol fluxes to stomatal conductance and leaf development). *Plant Physiology*, *108*, 1359–1368. https://doi.org/10.1104/pp.108.4.1359

Nightingale, P. D., Malin, G., Law, C. S., Watson, A. J., Liss, P. S., Liddicoat, M. I., et al. (2000). In situ evaluation of air-sea gas exchange parameterizations using novel conservative and volatile tracers. *Global Biogeochemical Cycles*, *14*, 373–387. https://doi.org/10.1029/1999GB900091

Olivier, J. G. J., Bouwman, A. F., Vandermaas, C. W. M., & Berdowski, J. J. M. (1994). Emission Database for Global Atmospheric Research (EDGAR). *Environmental Monitoring and Assessment*, *31*, 93–106.

Orlando, J. J., & Tyndall, G. S. (2012). Laboratory studies of organic peroxy radical chemistry: An overview with emphasis on recent issues of atmospheric significance. *Chemical Society Reviews*, *41*, 6294–6317.

Paulot, F., Wunch, D., Crounse, J. D., Toon, G. C., Millet, D. B., DeCarlo, P. F., et al. (2011). Importance of secondary sources in the atmospheric budgets of formic and acetic acids. *Atmospheric Chemistry and Physics*, *11*, 1989–2013. https://doi.org/10.5194/acp-11-1989-2011

Potter, C. S., Randerson, J. T., Field, C. B., Matson, P. A., Vitousek, P. M., Mooney, H. A., & Klooster, S. A. (1993). Terrestrial ecosystem production: A process model based on global satellite and surface data. *Global Biogeochemical Cycles*, *7*, 811–841. https://doi.org/10.1029/93GB02725

Ramachandran, A., & Walsh, D. A. (2015). Investigation of XoxF methanol dehydrogenases reveals new methylotrophic bacteria in pelagic marine and freshwater ecosystems. *FEMS Microbiology Ecology*, *91*, fiv105. https://doi.org/10.1093/femsec/fiv105

Randerson, J. T., Chen, Y., van der Werf, G. R., Rogers, B. M., & Morton, D. C. (2012). Global burned area and biomass burning emissions from small fires. *Journal of Geophysical Research*, *117*, G04012. https://doi.org/10.1029/2012JG002128

Randerson, J. T., Thompson, M. V., Conway, T. J., Fung, I. Y., & Field, C. B. (1997). The contribution of terrestrial sources and sinks to trends in the seasonal cycle of atmospheric carbon dioxide. *Global Biogeochemical Cycles*, *11*, 535–560. https://doi.org/10.1029/97GB02268

Read, K. A., Carpenter, J., Arnold, S. R., Beale, R., Nightingale, P. D., Hopkins, J. B., et al. (2012). Multi-annual observations of acetone, methanol and acetaldehyde in remote tropical atlantic air: Implications for atmospheric OVOC budgets and oxidative capacity. *Environmental Science & Technology*, *46*, 11028–11039. https://doi.org/10.1021/es302082p

Rinsland, C. P., Mahieu, E., Chiou, L., & Herbin, H. (2009). First ground-based infrared solar absorption measurements of free tropospheric methanol (CH_3OH): Multidecade infrared time series from Kitt Peak (31.9°N 111.6°W): Trend, seasonal cycle, and comparison with previous measurements. *Journal of Geophysical Research*, *114*, D04309. https://doi.org/10.1029/2008JD011003

Ruuskanen, T. M., Müller, M., Schnitzhofer, R., Karl, T., Graus, M., Bamberger, I., et al. (2011). Eddy covariance VOC emission and deposition fluxes above grassland using PTR-TOF. *Atmospheric Chemistry and Physics*, *11*, 611–625. https://doi.org/10.5194/acp-11-611-2011

Safieddine, S. A., Heald, C. L., & Henderson, B. H. (2017). The global nonmethane reactive organic carbon budget: A modeling perspective. *Geophysical Research Letters*, *44*, 3897–3906. https://doi.org/10.1002/2017GL072602

Sander, S. P., Friedl, R. R., Golden, D. M., Kurylo, M. J., Moortgat, G. K., Wine, P. H., et al. (2006). *Chemical kinetics and photochemical data for use in atmospheric studies: Evaluation number 15*. JPL Publication 02–25. Pasadena: Jet Propulsion Laboratory.

Sargeant, S. L., Murrell, J. C., Nightingale, P. D., & Dixon, J. L. (2016). Seasonal variability in microbial methanol utilisation in coastal waters of the western English Channel. *Marine Ecology Progress Series*, *550*, 53–64. https://doi.org/10.3354/meps11705

Sherwen, T., Evans, M. J., Carpenter, L. J., Andrews, S. J., Lidster, R. T., Dix, B., et al. (2016). Iodine's impact on tropospheric oxidants: A global model study in. GEOS-Chem. *Atmospheric Chemistry and Physics*, *16*(2), 1161–1186. https://doi.org/10.5194/acp-16-1161-2016

Sherwen, T., Schmidt, J. A., Evans, M. J., Carpenter, L. J., Großmann, K., Eastham, S. D., et al. (2016). Global impacts of tropospheric halogens (Cl, Br, I) on oxidants and composition in GEOS-Chem. *Atmospheric Chemistry and Physics*, *16*, 12239–12271. https://doi.org/10.5194/acp-16-12239-2016

Simpson, I. J., Akagi, S. K., Barletta, B., Blake, N. J., Choi, Y., Diskin, G. S., et al. (2011). Boreal forest fire emissions in fresh Canadian smoke plumes: C_1-C_{10} volatile organic compounds (VOCs), CO_2, CO, NO_2, NO, HCN and CH_3CN. *Atmospheric Chemistry and Physics*, *11*(13), 6445–6463. https://doi.org/10.5194/acp-11-6445-2011

Singh, H. B., Chen, Y., Tabazadeh, A., Fukui, Y., Bey, I., Yantosca, R., et al. (2000). Distribution and fate of selected oxygenated organic species in the troposphere and lower stratosphere over the Atlantic. *Journal of Geophysical Research*, *105*, 3795–3805. https://doi.org/10.1029/1999JD900779

Singh, H. B., Tabazadeh, A., Evans, M. J., Field, B. D., Jacob, D. J., Sachse, G., et al. (2003). Oxygenated volatile organic chemicals in the oceans: Inferences and implications based on atmospheric observations and air-sea exchange models. *Geophysical Research Letters*, *30*, 1862. https://doi.org/10.1029/2003GL017933

Sinha, P., Hobbs, P. V., Yokelson, R. J., Bertschi, I. T., Blake, D. R., Simpson, I. J., et al. (2003). Emissions of trace gases and particles from Savanna fires in southern Africa. *Journal of Geophysical Research*, *108*(D13), 8487. https://doi.org/10.1029/2002JD002325

Sinha, P., Hobbs, P. V., Yokelson, R. J., Blake, D. R., Gao, S., & Kirchstetter, T. W. (2004). Emissions from miombo woodland and dambo grassland savanna fires. *Journal of Geophysical Research*, *109*(D11), 305. https://doi.org/10.1029/2004JD004521

Stavrakou, T., Guenther, A., Razavi, A., Clarisse, L., Clerbaux, C., Coheur, P.-F., et al. (2011). First space-based derivation of the global atmospheric methanol emission fluxes. *Atmospheric Chemistry and Physics*, *11*, 4873–4898. https://doi.org/10.5194/acp-11-4873-2011

Talbot, R., Mao, H. T., & Sive, B. (2005). Diurnal characteristics of surface level O_3 and other important trace gases in New England. *Journal of Geophysical Research*, *110*, D09307. https://doi.org/10.1029/2004JD005449

Thames, A. B., Brune, W. H., Miller, D. O., Allen, H. M., Apel, E. C., Blake, D. R., et al. (2020). Missing OH reactivity in the global marine boundary layer. *Atmospheric Chemistry and Physics*, *20*, 4013–4029. https://doi.org/10.5194/acp-20-4013-2020

Tie, X., Guenther, A., & Holland, E. (2003). Biogenic methanol and its impacts on tropospheric oxidants. *Geophysical Research Letters*, *30*, 1881. https://doi.org/10.1029/2003GL017167

Travis, K. R., Heald, C. L., Allen, H. M., Apel, E. C., Arnold, S. R., Blake, D. R., et al. (2020). Constraining remote oxidation capacity with ATom observations. *Atmospheric Chemistry and Physics*, *20*, 7753–7781. https://doi.org/10.5194/acp-20-7753-2020

Tyndall, G. S., Cox, R. A., Granier, C., Lesclaux, R., Moortgat, G. K., Pilling, M. J., et al. (2001). Atmospheric chemistry of small organic peroxy radicals. *Journal of Geophysical Research*, *106*, 12157–12182. https://doi.org/10.1029/2000JD900746

Vaida, V. (2011). Perspective: water cluster mediated atmospheric chemistry. *Journal of Chemical Physics*, *135*, 020901. https://doi.org/10.1063/1.3608919

van der Werf, G. R., Randerson, J. T., Giglio, L., Collatz, G. J., Mu, M., Kasibhatla, P. S., et al. (2010). Global fire emissions and the contribution of deforestation, savanna, forest, agricultural, and peat fires (1997-2009). *Atmospheric Chemistry and Physics*, *10*, 11707–11735. https://doi.org/10.5194/acp-10-11707-2010

Velasco, E., Pressley, S., Grivicke, R., Allwine, E., Coons, T., Foster, W., et al. (2009). Eddy covariance flux measurements of pollutant gases in urban Mexico city. *Atmospheric Chemistry and Physics*, *9*, 7325–7342. https://doi.org/10.5194/acp-9-7325-2009

von Dahl, C. C., Hävecker, M., Schlögl, R., & Baldwin, I. T. (2006). Caterpillar-elicited methanol emission: a new signal in plant–herbivore interactions? *Plant Journal*, *46*, 948–960. https://doi.org/10.1111/j.1365-313X.2006.02760.x

von Kuhlmann, R., Lawrence, M. G., Crutzen, P. J., & Rasch, P. J. (2003). A model for studies of tropospheric ozone and nonmethane hydrocarbons: model evaluation of ozone-related species. *Journal of Geophysical Research*, *108*, 4729. https://doi.org/10.1029/2002JD003348

Wang, S., Apel, E. C., Schwantes, R. H., Bates, K. H., Jacob, D. J., Fischer, E. V., et al. (2020). Global atmospheric budget of acetone: Air-sea exchange and the contribution to the hydroxyl radicals. *Journal of Geophysical Research: Atmospheres*, *125*(15), e2020JD032553.

Wang, S., Hornbrook, R. S., Hills, A., Emmons, L. K., Tilmes, S., Lamarque, J.-F., et al. (2019). Atmospheric acetaldehyde: importance of air-sea exchange and a missing source in the remote troposphere. *Geophysical Research Letters*, *46*, 5601–5613. https://doi.org/10.1029/2019GL082034

Wang, Y., Logan, J. A., & Jacob, D. J. (1998). Global simulation of tropospheric O_3-NO_x-hydrocarbon chemistry: 2. Model evaluation and global ozone budget. *Journal of Geophysical Research*, *103*, 10727–10755. https://doi.org/10.1029/98JD00157

Warneke, C., Bahreini, R., Brioude, J., Brock, C. A., de Gouw, J. A., Fahey, D. W., et al. (2009). Biomass burning in Siberia and Kazakhstan as an important source for haze over the Alaskan Arctic in April 2008. *Geophysical Research Letters*, *36*(L02), 813. https://doi.org/10.1029/2008GL036194

Warneke, C., Karl, T., Judmaier, H., Hansel, A., Jordan, A., Lindinger, W., & Crutzen, P. (1999). Acetone, methanol, and other partially oxidized volatile organic emissions from dead plant matter by abiological processes: Significance for atmospheric HO_x chemistry. *Global Biogeochemical Cycles*, *13*, 9–17. https://doi.org/10.1029/98GB02428

Warneke, C., McKeen, S. A., de Gouw, J. A., Goldan, P. D., Kuster, W. C., Holloway, J. S., et al. (2007). Determination of urban volatile organic compound emission ratios and comparison with an emissions database. *Journal of Geophysical Research*, *112*, D10S47. https://doi.org/10.1029/2006JD007930

Wells, K. C., Millet, D. B., Cady-Pereira, K. E., Shephard, M. W., Henze, D. K., Bousserez, N., et al. (2014). Quantifying global terrestrial methanol emissions using observations from the TES satellite sensor. *Atmospheric Chemistry and Physics*, *14*, 2555–2570. https://doi.org/10.5194/acp-14-2555-2014

Wells, K. C., Millet, D. B., Hu, L., Cady-Pereira, K. E., Xiao, Y., Shephard, M. W., et al. (2012). Tropospheric methanol observations from space: retrieval evaluation and constraints on the seasonality of biogenic emissions. *Atmospheric Chemistry and Physics*, *12*, 5897–5912. https://doi.org/10.5194/acp-12-5897-2012

Wennberg, P. O., Bates, K. H., Crounse, J. D., Dodson, L. G., McVay, R. C., Mertens, L. A., et al. (2018). Gas-phase reactions of isoprene and its major oxidation products. *Chemistry Review*, *118*, 3337–3390. https://doi.org/10.1021/acs.chemrev.7b00439

Wentworth, G. R., Aklilu, Y.-A., Landis, M. S., & Hsu, Y.-M. (2018). Impacts of a large boreal wildfire on ground level atmospheric concentrations of PAHs, VOCs and ozone. *Atmospheric Environment*, *178*, 19–30. https://doi.org/10.1016/j.atmosenv.2018.01.013

Williams, J., Holzinger, R., Gros, V., Xu, X., Atlas, E., & Wallace, D. W. R. (2004). Measurements of organic species in air and seawater from the tropical Atlantic. *Geophysical Research Letters*, *31*, L23S06. https://doi.org/10.1029/2004GL020012

Wohl, C., Brown, I., Kitidis, V., Jones, A. E., Sturges, W. T., Nightingale, P. D., & Yang, M. (2020). Underway seawater and atmospheric measurements of volatile organic compounds in the Southern Ocean. *Biogeosciences*, *17*, 2593–2619. https://doi.org/10.5194/bg-17-2593-2020

Wohlfahrt, G., Amelynck, C., Ammann, C., Arneth, A., Bamberger, I., Goldstein, A. H., et al. (2015). An ecosystem-scale perspective of the net land methanol flux: Synthesis of micrometeorological flux measurements. *Atmospheric Chemistry and Physics*, *15*, 7413–7427. https://doi.org/10.5194/acp-15-7413-2015

Yan, C., & Krasnoperov, L. N. (2019). Pressure-dependent kinetics of the reaction between CH_3O_2 and OH: TRIOX formation. *Journal of Physical Chemistry A*, *123*, 8349–8357. https://doi.org/10.1021/acs.jpca.9b03861

Yan, C., Kocevska, S., & Krasnoperov, L. N. (2016). Kinetics of the reaction of CH_3O_2 radicals with OH studied over the 292-526 K temperature range. *Journal of Physical Chemistry A*, *120*, 6111–6121. https://doi.org/10.1021/acs.jpca.6b04213

Yang, M., Beale, R., Liss, P., Johnson, M., Blomquist, B., & Nightingale, P. (2014). Air-sea fluxes of oxygenated volatile organic compounds across the Atlantic Ocean. *Atmospheric Chemistry and Physics*, *14*, 7499–7517. https://doi.org/10.5194/acp-14-7499-2014

Yang, M., Blomquist, B. W., & Nightingale, P. D. (2014). Air-sea exchange of methanol and acetone during HiWinGS: Estimation of air phase, water phase gas transfer velocities. *Journal of Geophysical Research: Oceans*, *119*, 7308–7323. https://doi.org/10.1002/2014JC010227

Yang, M., Nightingale, P. D., Beale, R., Liss, P. S., Blomquist, B., & Fairall, C. (2013). Atmospheric deposition of methanol over the Atlantic Ocean. *Proceedings of the National Academy of Sciences of the United States of America*, *110*, 20034–20039. https://doi.org/10.1073/pnas.1317840110

Zhuang, J., Jacob, D. J., & Eastham, S. D. (2018). The importance of vertical resolution in the free troposphere for modeling intercontinental plumes. *Atmospheric Chemistry and Physics*, *18*, 6039–6055. https://doi.org/10.5194/acp-18-6039-2018